Earth Syst. Sci. Data Discuss., https://doi.org/10.5194/essd-2019-73
Manuscript under review for journal Earth Syst. Sci. Data
Discussion started: 22 May 2019

The Cumulus And Stratocumulus CloudSat-CALIPSO Dataset (CASCCAD)

Grégory Cesana[1,2], Anthony D. Del Genio[2] and Hélène Chepfer[3,4]

[1] Columbia University, Center for Climate Systems Research, Earth Institute, New York, NY, USA
[2] NASA Goddard Institute for Space Studies, New York, NY, USA
[3] LMD/IPSL, Sorbonne Université, Paris, France
[4] LMD/IPSL, CNRS, École Polytechnique, Palaiseau, France

Correspondence to: Gregory V. Cesana (Gregory.cesana@columbia.edu)

Abstract.

Low clouds continue to contribute greatly to the uncertainty in cloud feedback estimates. Depending on whether a region is dominated by cumulus (Cu) or stratocumulus (Sc) clouds, the interannual low-cloud feedback is somewhat different in both space-borne and large eddy simulation studies. Therefore, simulating the correct amount and variation of the Cu and Sc cloud distributions could be crucial to predict future cloud feedbacks. Here we document spatial distributions and profiles of Sc and Cu clouds derived from Cloud-Aerosols Lidar and Infrared Pathfinder Satellite Observations (CALIPSO) and CloudSat measurements. For this purpose, we create a new dataset called the Cumulus And Stratocumulus CloudSat-CAlipso Dataset (CASCCAD). To separate the Cu from Sc, we design an original method based on the cloud height, horizontal extent and vertical variability, which is applied to both CALIPSO and combined CloudSat-CALIPSO observations. First, the choice of parameters used in the discrimination algorithm is investigated and validated in selected Cu, Sc and and Sc-Cu transition case studies. Then, the global statistics are compared against those from existing passive and active-sensor satellite observations. Our results indicate that the cloud optical thickness –as used in passive-sensor observations– is not a sufficient parameter to discriminate Cu from Sc clouds, in agreement with previous literature. On the contrary, classifying Cu and Sc clouds based on their geometrical shape leads to spatial distributions consistent with prior knowledge of these clouds, from ground-based, ship-based and field campaigns. Furthermore, we show that our method improves existing Sc-Cu classification by using additional information on cloud height and vertical cloud fraction variation. Finally, the CASCCAD datasets provide a basis to evaluate shallow convection (Cu) and boundary layer (Sc) clouds on a global scale in climate models and potentially improve our understanding of low-level cloud feedbacks. The CASCCAD dataset (Cesana, 2019, DOI: http://doi.org/10.5281/zenodo.2667637) is available on the Goddard Institute for Space Studies (GISS) website at https://data.giss.nasa.gov/clouds/casccad/ and on zenodo website at https://zenodo.org/record/2667637.

Earth Syst. Sci. Data Discuss., https://doi.org/10.5194/essd-2019-73
Manuscript under review for journal Earth Syst. Sci. Data
Discussion started: 22 May 2019

1 Introduction

Whether clouds will amplify or dampen global warming, referred to as cloud feedbacks, continues to be a dominant source of uncertainty in future climate projections, for which low clouds over the tropics and at mid-latitudes contribute up to 50 % in recent generations of the Coupled Model Intercomparison Project (CMIP) models (Zelinka et al., 2016). Low clouds (i.e., cloud top height lower than ~ 3 km) may be separated into two main categories: stratocumulus (Sc, including stratus clouds) and cumulus (Cu). Since these clouds are governed by distinct processes, they are likely to respond differently to climate warming (i.e., Bretherton, 2015). Driven by radiative cooling, Sc clouds cap the planetary boundary layer over cool oceans in conditions with a strong cloud top inversion, mostly off the western coasts of continents (e.g., Klein and Hartmann, 2002). They are typically hundreds of meters thick with a large horizontal extent, which can be either homogeneous (in decks) or heterogenous (open and closed cells), and a stable cloud-top height. Due to their large cloud cover, these clouds strongly reflect shortwave (SW) radiation and contribute to surface cooling. As the ocean warms up further west in the trade-wind regions, the latent heat flux increases and the convection becomes surface driven, therefore favoring breaking up of Sc and the subsequent formation of Cu clouds (Albrecht et al., 2019; Wyant et al., 1997). These clouds are horizontally limited and scattered – i.e., with a modest cloud cover – and their tops can rise above the PBL. Since these low clouds are governed by distinct processes, they may respond differently to climate warming and there is no fundamental reason to expect the two cloud types to exhibit the same feedback.

Idealized large-eddy simulation (LES) studies have partly supported the hypothesis of different cloud type responses to climate warming, i.e., a substantial decrease of Sc as opposed to a moderate decrease to no change for Cu, yet, the underlying processes remain poorly understood, particularly for trade-wind Cu (Bretherton, 2015). Furthermore, recent satellite-based studies have shown that the interannual low-cloud feedback in response to SST forcings is somewhat different depending on whether a region is dominated by Cu or Sc clouds (Cesana et al., 2019a; McCoy et al., 2017). Therefore, simulating the right amount of Cu and Sc clouds could be crucial for models to reproduce the overall interannual low-cloud feedback as observed from space (Cesana et al., 2019a) and to predict future cloud feedbacks (Klein and Hall, 2015). Yet the relatively scarce amount of observations that fundamentally distinguish Sc and Cu clouds (mostly field campaigns and ground-based sites, i.e, Zhou et al., 2015; Rémillard et al., 2012) limits our ability to study the present-day global distribution of these clouds and their response to surface warming, and hence to better constrain the climate models.

Estimating the global radiative impact of clouds on past, present and future climate continues to be a challenging question that requires observations of cloud macrophysical (e.g., height, spatial extent) and microphysical (e.g., phase, effective radius) properties on a global scale. Knowledge of the cloud type provides only a little leverage on determining their radiative

Earth Syst. Sci. Data Discuss., https://doi.org/10.5194/essd-2019-73
Manuscript under review for journal Earth Syst. Sci. Data
Discussion started: 22 May 2019

properties, which may explain why cloud-type classification has received far less attention in the past. The first global-scale cloud-type observations were collected visually from land stations and ships in the 1950s and were subsequently compiled to make a coarse digital database in the late 1980s (Hahn et al., 1988) and were updated a couple of decades after (Hahn and Warren, 2007). A few years later, the first global-scale cloud type climatology derived from passive-sensor satellites emerged, based on cloud top pressure (CTP) and cloud optical thickness (COT) (Rossow and Schiffer, 1991, 1999). While very useful because of its long-time record, large spatial cover and finer resolution than Hahn et al. (1988), such datasets suffer from both methodology and instrumental limitations that make it difficult to fully discriminate Sc from Cu clouds. The CTP-COT method does not exploit information on the spatial shape of the cloud, that is to say its horizontal and vertical extent, and thus is not always accurate (Hahn et al., 2001; Pincus et al., 1999). Additionally, passive-sensor satellites do not describe the entire profile but only the uppermost layers, integrated over a height that is moreover hard to quantify with less confidence over land and in regions of strong inversion (Garay et al., 2008; Marchand et al., 2010). Thus, low cloud cover in regions of extensive higher clouds is underestimated. Finally, some instruments may not be well-suited for Cu cloud detection (Marchand et al., 2010).

By combining collocated observations from active CloudSat Cloud Profiling Radar (CPR, Stephens et al., 2002) and Cloud-Aerosols Lidar and Infrared Pathfinder Satellite Observations (CALIPSO; Winker et al., 2010) lidar and passive Moderate Resolution Imaging Spectroradiometer (MODIS; King et al., 2013) spectrometer, the 2B-CLDCLASS-LIDAR product (Sassen and Wang, 2008; Wang et al., 2013) addresses most of the above caveats. It classifies clouds into eight types based on cloud vertical and horizontal extent, reflectivity, precipitating state, temperature, height and brightness (Huang et al., 2015). However, this combined dataset is only available for a relatively short period of time (about 4.5 years), which influences statistical correlations between environment variables and cloud fraction (e.g., Cesana et al., 2019a; Klein et al., 2017). Although the radar-only product extends over a longer time-period (for daytime only, see section 2.2), the CPR is less sensitive to fractionated and thin shallow cumulus clouds than the CALIPSO lidar and its ground clutter prevents cloud detection below 1 km, which includes a large portion of Sc and Cu clouds. Furthermore, the CPR horizontal resolution (~ 1.4 km x 1.1 km) is not ideal for shallow cumulus detection, which are typically smaller than 1 km (Rodts et al., 2003; Zhang and Klein, 2013). Therefore, creating a specific Sc-Cu cloud classification product based on CALIPSO observations only would allow one to overcome these issues although confining the analysis to regions with optically thin or no overlying high-clouds.

Here we propose to document spatial distributions and profiles of Sc and Cu clouds derived from CALIPSO measurements. To achieve this goal, we create an original method based on the cloud height, horizontal extent and vertical variability, which can be applied to both CALIPSO and combined CloudSat-CALIPSO observations, referred to as the Cumulus And Stratocumulus CloudSat-CAlipso Dataset (CASCCAD, Cesana, 2019; DOI: http://doi.org/10.5281/zenodo.2667637). The datasets are presented in section 2. The sensitivity of the CASCCAD algorithm is assessed in section 3 and the global-scale results are then discussed and compared to a subset of existing cloud-type datasets in section 4. Finally, section 5 summarizes the results.

Earth Syst. Sci. Data Discuss., https://doi.org/10.5194/essd-2019-73
Manuscript under review for journal Earth Syst. Sci. Data
Discussion started: 22 May 2019

2 Datasets

2.1 GOCCP

The instantaneous cloud mask of the GCM-oriented CALIPSO Cloud Product (GOCCP) version 3.1.2 (Guzman et al., 2017) is used by our discrimination algorithm (referred to as DA, described in section 3.2) to derive Sc-Cu cloud fraction statistics from 2007 to 2016 over a 2.5˚ grid and for 40 levels with 480 m spacing from 0 to 19.2 km. GOCCP (Chepfer et al., 2010) was developed to facilitate the evaluation of cloud properties in GCMs when combined with a lidar simulator (Chepfer et al., 2008) that uses the same cloud definitions, and ensures a consistent comparison between observations and simulations (Cesana and Waliser, 2016). The ratio of the Total Attenuation Backscatter signal (ATB) to the molecular ATB – so-called Scattering Ratio (SR) – is computed from the level1B CALIPSO files for every 333 m-along-track-resolution near-nadir lidar profile for 480 m height intervals. This lidar-based quantity is a proxy of the presence of particulate matter in a layer. GOCCP uses a fixed SR threshold to detect clouds (SR>5), for either daytime or nighttime data, regardless of the vertical level. This threshold allows the detection of thin cirrus cloud in the high-troposphere (McGill et al., 2007), hence the majority – if not all – of optically thicker PBL clouds except when masked by overlying high-clouds (e.g., the trade-wind regions). It also prevents most false detections of aerosol layers as being cloudy in the PBL (Chepfer et al., 2013). GOCCP has been validated against in situ (Cesana et al., 2016) and ground-based observations (Lacour et al., 2017). Caveats for this dataset are discussed in Cesana et al. (2016) and in Cesana and Waliser (2016). Compared to GOCCP version 2.9 (Cesana et al., 2016), version 3.1.2 improves the detection of fully attenuated pixels by introducing a surface echo detection. When no lidar echo is detected, pixels below the lowest cloudy pixel are diagnosed as being fully attenuated and therefore not accounted for in the cloud fraction computation. This new feature reduces the underestimation of the cloud fraction underneath optically thick liquid-topped clouds in the lower troposphere (Cesana et al., 2016).

2.2 CloudSat-CALIPSO RL-GeoProf

Additionally, the Sc-Cu DA is applied to combined CloudSat-CALIPSO profiles (using the radar-lidar geometrical profile product [RL-GeoProf], Mace and Zhang, 2014; version R04) from 2007 to 2010 over a 2.5˚ grid and for 80 levels with 240 m spacing from 0 to 19.2 km. From its launch to early April 2011, CloudSat flew approximately 15 s ahead of CALIPSO making it possible to observe the same scene from a lidar-radar perspective when using both the 2B-GEOPROF and 2B-GEOPROF-LIDAR products (Mace and Zhang, 2014). CloudSat experienced a severe anomaly in April 2011, which forced the satellite to leave the A-Train constellation before coming back in June 2012 in "Daylight Only Operation mode" (DO-Op). As a result, CloudSat-CALIPSO combined observations are only available for 4.5 years. The CPR cloud mask provides confidence levels for the cloud detection (Marchand et al., 2009). Following Mace and Zhang (2014), we chose the confidence level of 20 and higher to characterize the presence of a cloud from the radar cloud mask. The CPR has a coarser horizontal (~ 1.4 km x 1.1 km) and vertical resolution (240 m) than the CALIPSO lidar (Δz = 30 m below 8 km and 60 m above 8 km for ~ 70 m footprint every 333 m). As a result, several lidar profiles fall within the CloudSat radar footprint most of the time. These are used to

Earth Syst. Sci. Data Discuss., https://doi.org/10.5194/essd-2019-73
Manuscript under review for journal Earth Syst. Sci. Data
Discussion started: 22 May 2019

compute the lidar cloud fraction (CF_{lidar}, from 0 to 1) based on the CALIPSO Vertical Feature Mask (VFM) of the level2 5km CALIPSO files (Vaughan et al., 2009), at the CPR resolution in the 2B-GEOPROF-LIDAR files. While the CF_{lidar} can sometimes be lower than 0.5, we kept the 0.5 threshold to diagnose the presence of a cloud as in Mace and Zhang (2014) and Cesana et al. (2019b). Diagnosing a pixel as cloudy from values below 0.5 may result in an overestimate of the averaged cloud fraction when compared to ground-based measurements (Fig. S1 and Marchand et al., 2010).

2.3 2B-CLDCLASS-LIDAR

The 2B-CLDCLASS-LIDAR product (Sassen and Wang, 2008; referred to as 2BCCL in the remainder of the manuscript) merges collocated observations from the CloudSat CPR, CALIPSO lidar and MODIS spectrometer to classify clouds into eight types based on several criteria: their vertical and horizontal extent, their precipitating state, their temperature, and their radiance. Although eight cloud types are available in this dataset (Deep convective, Cirrus, Nimbostratus, Altostratus, Altocumulus, Cumulus including fair-weather and congestus, Stratus and Stratocumulus), we only focus on the Cu, stratus (St) and Sc cloud-types. The St and Sc cloud-types are combined into a single category referred to as Sc for consistency with the Sc-Cu discrimination algorithm, which does not differentiate these two categories. In addition, the Sc and St clouds are particularly difficult to distinguish in the 2BCCL product because of the ground clutter contamination in the radar signal (Sassen and Wang, 2008) as shown by Huang et al. (2015). In 2BCCL, the cloud base and top are given for up to ten cloudy layers, which is why we re-project these cloudy layers onto a 480 m vertical grid from 0 to 19.2 km to be consistent with the GOCCP and RL-GeoProf datasets described in sections 2.1 and 2.2. Those are then accumulated into a 2.5˚x2.5˚ grid as for the two other products.

3 Description of The Cumulus And Stratocumulus CloudSat-CAlipso Dataset (CASCCAD) discrimination algorithm

3.1 Why choose GOCCP and CloudSat-CALIPSO RL-GeoProf?

The main goal of this study is to document spatial distributions and profiles of Sc and Cu clouds on a global scale, with the desire to further analyze long-term relationships between Sc-Cu clouds and environmental parameters in future studies. For this purpose, we need to i) distinguish the two cloud types based on observable cloud-properties and ii) use datasets that are available for a time-period sufficiently long (~ 10 years) to compute statistically significant relationships (e.g., using 4 years of GOCCP rather than 10 may decrease the amplitude of the relationship between low clouds and SST anomalies by more than 15 %, Cesana et al., 2019a). Although both the Sc and Cu clouds form within the planetary boundary layer (PBL), they have relatively different shapes as they are controlled by different physical mechanisms. The Cu (Fig. 1, second to last column) can stretch up past the PBL into the lower free troposphere (z ~ 3 km) while they have typically a small horizontal extent (no more than a few km, e.g, Lamer et al., 2015; Nuijens et al., 2015b). On the contrary, the Sc (Fig. 1, first column) have a relatively small vertical extent (no more than a few hundred meters) and a cloud-top height (CTH) controlled by the PBL depth but spread out over tens to hundreds of kilometers (Wood, 2012) either homogeneously or heterogeneously (open-cell). In

Earth Syst. Sci. Data Discuss., https://doi.org/10.5194/essd-2019-73
Manuscript under review for journal Earth Syst. Sci. Data
Discussion started: 22 May 2019

between, these two distinct regimes, various transitioning clouds may form (Albrecht et al., 2019; Teixeira et al., 2011) and the most frequent are: broken Sc and transitioning Sc-Cu, which is composed of Cu under Sc (Albrecht et al., 2019, Rauber et al., 2007) and Cu with stratiform outflow (Lamer et al., 2015, Nuijens et al., 2015b) (Fig. 1, second to fourth column, respectively). Clouds with a cloud base and a cloud top within and outside the lower free troposphere, respectively, are classified as deep Cu (Fig. 1, last column). Bearing the above facts in mind, we design the CASCCAD DA based on cloud height and vertical and horizontal cloud fraction, which can be applied to both GOCCP instantaneous profiles and the CloudSat-CALIPSO level 2 geometrical profile product (referred to as RL-GeoProf).

GOCCP instantaneous profiles satisfy the criteria i) and ii) mentioned above. They use all 70-m-large lidar shots every 333 m along-track without horizontal averaging, which allows the detection of the geometrically sparsest shallow Cu, besides the more horizontally extended Sc, over a relatively extended time-period (from June 2006 to 2017, while CALIPSO is still operating as of April 2019). This decadal dataset makes it possible to analyze climatological values of Cu and Sc cloud fraction and their relationships to environmental parameters. However, as the lidar penetrates within cloudy layers, the signal eventually attenuates completely for optical thickness greater than 3 to 5. Therefore, it is not always possible to observe the full troposphere with a space-borne lidar, which may cause differences in satellite-based cloud climatologies obtained from different instruments (Kikuchi et al., 2017; Thorsen et al., 2013). In these instances –i.e., in deep convective clouds or in the storm tracks–, the CPR capability complements cloud profiles beneath the height at which the lidar attenuates, although the CPR clutter prevents using CloudSat data below ~ 1000 m. Unfortunately, the RL-GeoProf product is only available for a short period of time (~ 4.5 years) due to the severe anomaly of April 2011, which is why CloudSat-CALIPSO observations satisfy i) but only partially ii).

3.2 First criterion of the discrimination algorithm: the cloud-top height

As mentioned above, three main criteria –represented by different colors in Fig. 2– are used in the DA to separate Sc from Cu clouds and to characterize the various Sc-Cu transitioning clouds presented in Fig.2: the CTH, the Horizontal Cloud Fraction (HCF) and the Vertical Cloud Fraction (VCF). Note that the sensitivity to these criteria is later tested in section 4.1. The first step of the DA depends on the height of the cloud top (Fig. 2, 1st column, in grey). Because trade Cu and Sc are low clouds, their CTH must be within the lower free troposphere, which is defined as 3.36 km in GOCCP (approximately equivalent to the 680-hPa definition of Rossow and Schiffer, 1999). Furthermore, since Sc clouds cap the PBL, their CTH is typically lower than the PBL height over the main Sc deck areas, i.e., ~ 2 km (Albrecht et al., 1995; Bretherton et al., 2010; Garay et al., 2008; Wood, 2012; Zhou et al., 2015; Zuidema et al., 2009). Therefore, all cloud layers –i.e., a vertically-contiguous group of cloudy 480-m-pixels– with a cloud top higher than 1.92 km, which is the closest 480-m GOCCP level to 2 km, are diagnosed as Cu type. We remind the reader that the sensitivity of the algorithm to this criterion, as well as the other criteria, is tested in section 4.1.

Earth Syst. Sci. Data Discuss., https://doi.org/10.5194/essd-2019-73
Manuscript under review for journal Earth Syst. Sci. Data
Discussion started: 22 May 2019

3.3 Second criterion: the horizontal cloud fraction

The remaining clouds are passed to the second step of the DA (Fig. 2, 2nd column, in orange), which computes the HCF either centered around the lidar profiles (CHCF) or using forward (FHCF) or backward profiles (BHCF) as shown in Fig. 3. These three HCFs ensure capturing the full horizontal extent of the cloud layer regardless of whether the lidar probes toward the edge or the center of the layer while remaining more computationally efficient than treating clouds by contiguous horizontal-clusters. For example, the CHCF is 100 % in the specific case of Fig. 3a whereas FHCF and BHCF are about 50 %. Should the first lidar profile be at the beginning of the cloud, the centered, forward and backward HCF would be about 53, 100 and 7 % (Fig. 3b). Additionally, the HCFs are computed over four different length scales, 10, 20, 40 and 80 km, to characterize various cloud scenarios: open-cell and closed-cell Sc (Wood, 2012), Sc-Cu transitioning clouds (Albrecht et al., 2019; Teixeira et al., 2011) and different Cu organizations (Lamer et al., 2015; Rauber et al., 2007). The larger 40-80-km scales permit a clear distinction between the two type of clouds since Sc clouds typically cover vast areas compared to more fractionated trade-Cu clouds. Figures 4c and 4d show the probability density function (PDF) of the 40-km and 80-km CHCFs, respectively, for typical Cu (light blue bars) and Sc (light red bars) cases extracted from day and night CALIPSO orbits over the tropics (35˚S/N, eight orbit segments in total). These results confirm a rather clear separation, marked by purple lines, between the two populations for CHCFs. Although some slight overlap is visible, it disappears when the 40 and 80-km CHCFs are run together (not shown). However, in regions of open-cell Sc and Sc-Cu transition, the overlap may be larger (Fig. S2) and additional tests are needed to determine the type of clouds, i.e., Sc, broken Sc, transitioning Sc-Cu or Cu. In those instances, the 10 and 20-km CHCFs help further distinguish Sc from the other clouds (Fig. 4a and 4b). Finally, note that when all 480-m-pixels below 1.92 km are fully attenuated, the profile is excluded from the HCF computation.

3.4 Third criterion: the vertical cloud fraction

The third step of the DA (which comes into play only if the first two criteria have ruled out a pure Cu cloud) utilizes the VCF, computed 80-km along track, to capture the transitioning Sc-Cu and broken Sc clouds (Fig. 2, 3rd column, in purple). Since Sc clouds are relatively shallow – no more than a few hundred meters (Wood, 2012) – any cloud layer with a substantial VCF over 3 levels or more (vertical extension greater than 1.44 km) is diagnosed as transitioning Sc-Cu while the rest are diagnosed as Sc. The VCF threshold (= 0.12) is defined as approximately two times the standard deviation of the PDF of the 40-km CHCF computed using each of the seven first levels (0 to 3.36 km) in typical Cu regions. Finally, this VCF test is also applied to any cloud layer that passes the 40 and 80-km HCFs thresholds, regardless of their 10 and 20-km HCFs. In these cases, the cloud type is diagnosed as transitioning Sc-Cu if the VCF threshold is met, otherwise the cloud layer is diagnosed as broken Sc.

3.5 Horizontal continuity test

Once the cloud type is determined, it is applied vertically to the whole cloudy layer. While the DA takes into account the horizontal extent of a cloud system via the computation of HCFs (including possible clear sky profiles), it does not track horizontally-contiguous clusters of clouds (without clear sky profiles). As a result, in Cu and transitioning Sc-Cu cases, the same horizontally-contiguous cloud layer may be diagnosed as both Sc and Cu (Fig. 5b), which is more likely a Cu with a stratiform outflow (Lamer et al., 2015). To avoid this "slicing" issue, we apply a horizontal continuity test, which first detects a horizontally-contiguous cluster of clouds and then turns it into a homogeneous Cu if one third of the cluster is diagnosed as Cu type. We chose this arbitrary threshold because, on average, the fraction of the Cu that expands further aloft (geometrically thicker) is typically smaller than that near the lifting condensation level (Nuijens et al., 2015a) or that detrained near the trade-wind inversion (Nuijens et al., 2015a, Lamer et al., 2015).

4 Results

4.1 Case studies

To assess our CASCCAD DA, we analyze a series of three typical case studies: trade cumulus, stratocumulus and stratocumulus-cumulus transitioning clouds. First, we investigate the sensitivity of the DA to some of the criteria presented in Section 3 using GOCCP observations: the HCF (more or less conservative), CTH (one level higher) and VCF (smaller threshold, divided by 2) thresholds and the continuity test (turned off). We then compare the results of the standard DA applied to GOCCP and RL-GeoProf against the 2BCCL cloud types –for the same case studies– and utilize the collocated MODIS reflectance to provide a broader context of the cloud scene.

4.1.1 Stratocumulus case

Figure 6 shows the sensitivity of the GOCCP Sc-Cu Mask (Fig. 6d) to the different parameters used in the DA (Fig. 6b-c-e-f-g) for a daytime orbit segment off the coast of California during summer (see Fig. S3 for the exact location). The refined CALIPSO Science-Team (CALIPSO-ST) cloud mask (Δz = 30 m; Vaughan et al., 2009) helps us get a better sense of the cloud geometrical thickness where the lidar is not fully attenuated (Fig. 6a, black color). Additionally, the MODIS true reflectance image confirms the presence of stratiform layers of clouds throughout the CALIPSO-CloudSat path (Fig. 7d). Except for the lower VCF parameters, which reduce the along-track Sc CF (HCF_{Sc}) by 6.4 % (absolute value, Fig. 6b), the HCF_{Sc} is quite insensitive to the DA parameters (HCF_{Sc} = 67.4 +2.2/-1.4 %). Reducing the VCF (Fig. 6b) turns the edges of the Sc decks into transitioning Sc - Cu clouds (around 16˚N and 20˚N). However, changing the HCF thresholds have limited effect on the HCF_{Sc} in this particular case (Fig. 6f and 6g).

GOCCP and RL-GeoProf have a similar HCF_{Sc} while that of the 2BCCL product is larger along with its total HCF (Fig. 7). The substantial difference between RL-GeoProf and 2BCCL total HCFs is mostly due to differences in lidar cloud fraction treatment. The lidar cloud fraction from RL-GeoProf comes from the CALIPSO 5km VFM mask, whereas that of 2BCCL comes from the Lidar-AUX product (Wang et al., 2013).

4.1.2 Cumulus case

Earth Syst. Sci. Data Discuss., https://doi.org/10.5194/essd-2019-73
Manuscript under review for journal Earth Syst. Sci. Data
Discussion started: 22 May 2019

As for the Sc case, the along-track Cu CF (HCF_{Cu}) is weakly sensitive to variations of the different DA parameters (Fig. 8, HCF_{Cu} = 23.6 +1.1/-1.5 %). The most sensitive parameter is the horizontal continuity (Fig. 8e). When activated, it captures most of the large Cu between 20˚S and 18˚S although its southernmost edge remains likely incorrectly diagnosed as Sc. Most of the other cloudy features are diagnosed as Cu except for the cloudy layer located between 31˚ and 29˚S, which seems to be stratiform judging from its geometrical thickness (Fig. 8a) and reflectance (Fig. 9d).

Here again, both GOCCP and RL-GeoProf diagnose similar Sc and Cu HCFs although the DA fully captures the aforementioned large Cu only when it is used with RL-GeoProf observations (Fig. 9b). Unlike the Sc case, GOCCP and RL-GeoProf disagree substantially with 2BCCL. For example, several cloud clusters are diagnosed as Sc by the 2BCCL algorithm although their geometrical thickness is larger than 1.5 km (Fig. 9c, around 34˚S, 19˚S and 12˚S), making it very unlikely that these clusters are actual Sc. As a result, the HCF_{Sc} (27.9 %) is larger than the HCF_{Cu} (22.6 %) and approximately five times larger than that of GOCCP and RL-GeoProf. In addition, it is important to note that the 2BCCL total HCF is ~35 % larger than that of RL-GeoProf for two reasons. Firstly, the 2BCCL algorithm is derived from a different version of the collocated lidar product (Wang et al., 2013). Secondly, no CF_{lidar} threshold is used, which may cause a slight overestimate of the cloud fraction, particularly in the low levels albeit to a smaller extent than the differences between the two lidar products. As a result, the low-level cloud fraction of the 2BCCL product may be largely overestimated over the tropical and subtropical oceans. This overestimation is supported by a comparison with ground-based data and other satellite products over the Barbados (more than 2 times larger, Fig. S1), a region dominated by trade cumulus clouds (Nuijens et al., 2015b). An additional Cu case, in the trade-dominated NW Atlantic, confirms the ability of the DA to correctly diagnose a field of purely Cu clouds with no Sc (Fig. 10a and 10b). As in Fig. 9c, the 2BCCL product classifies a non-negligible amount of the clouds as Sc (Fig. 10c, HCF_{Sc} = 6.8 %) and overestimates the HCF_{tot} compared to GOCCP and RL-GeoProf.

4.1.3 Cumulus and open stratocumulus case

The last case study extends from the subtropics to the extra-tropics. Such location allows us to characterize transitioning Sc-Cu cases, which includes Sc, open-Sc and Cu clouds (Fig. 11). A visual inspection of the CTH variation from the CALIPSO VFM (Fig. 11a) suggests that this orbit segment contains three distinct clusters of clouds: Sc from 55˚ to 43˚S and from 25˚ to 20˚S and Cu in between. These three distinct layers are quite well captured by the DA although the DA is more sensitive to changes in the parameters than in the other cases. The most sensitive parameters are the VCF and HCF thresholds. Reducing the VCF threshold (Fig. 11b) turns 7.9 % of the Sc into Cu (absolute value) mostly poleward of 43˚S because the BL height decreases, causing multiple levels to be cloudy and subsequently diagnosed as Cu. Choosing smaller HCF thresholds (Fig. 11g) increases the Sc amount by 5.3 % (absolute value). This converts the few Cu poleward 43˚S into Sc as well as some Cu around 24˚S, which could very well be “true” Sc.

The three clusters of clouds are also well captured in the RL-GeoProf dataset, which detects somewhat more Cu than GOCCP making the total HCF larger as well (Fig. 12). On the contrary, the 2BCCL product diagnoses nearly two times more Sc than the CASCCAD datasets and two to three times less Cu.

Earth Syst. Sci. Data Discuss., https://doi.org/10.5194/essd-2019-73
Manuscript under review for journal Earth Syst. Sci. Data
Discussion started: 22 May 2019

4.2 Statistical analysis

4.2.1 Maps

In this section, we analyze climatological geographical distributions of Sc and Cu clouds for the three products presented before as well as for a subset of passive-sensor observations. These include the International Satellite Cloud Climatology Project (ISCCP, Rossow and Schiffer, 1999), the Moderate Resolution Imaging Spectroradiometer (MODIS, King et al., 2013) and the Multi-Angle Imaging Spectroradiometer (MISR, Marchand et al., 2010) observations. Sc and Cu are separated using a cloud top pressure (CTP) - cloud optical thickness (COT) diagram introduced by Rossow and Schiffer (1999): CTP must be larger than 680hPa for each type and COT smaller or larger than 3.6 for Cu and Sc clouds, respectively. Note that this COT-based method has been shown to mis-classify Cu and Sc that have moderate optical thickness (e.g., Pincus et al., 1999). Passive-sensor estimates of Sc and Cu provide a broader context and help us emphasize the added value of new Sc-Cu discrimination methods based on active-sensor satellites.

Overall, all products identify quite well the large cloud fraction in the tropical and subtropical stratocumulus areas, off the west coast of the continents (Fig. 13, top row). RL-GeoProf and 2BCCL products detect the largest low-level cloud fraction (Fig. 14, zonal and global mean, top row) although they might overestimate the fractionated clouds (e.g., Cu), in particular 2BCCL –as shown in the case study analysis– because it uses a different version of the collocated lidar product. Unlike the passive-sensor products –based solely on the CTP and COT–, the active-sensor products do not detect significant amount of Cu off the western coasts of the continents compared to the large Sc cloud fraction, which ranges from 50 % off the coast of Australia up to 85 % in the heart of the deck off the coast of Peru in both GOCCP and RL-GeoProf (Fig. 13, third row). These results are somewhat different from previous analysis in which the Sc cloud fraction ranges from 40 to 60 % over the Sc deck areas (Wood, 2012). On the contrary, Additionally, the CASCCAD products place a substantial amount of Cu clouds west of Sc decks (up to 40 %) and in the trade-wind regions (between 20 and 30 %), similar to MISR observations (Fig. 13, third row), which is more sensitive to fractionated clouds than ISCCP and MODIS. Here again our findings somewhat contradict earlier results retrieving Sc clouds 20 % of the time in the trade-wind regions (Wood, 2012). Besides the Cu and Sc categories, the CASCCAD products have a third category referred to as transitional clouds (Fig. 13, fourth row), which is supposed to capture regions of transition between Cu and Sc clouds. As expected, these clouds are located between Sc decks and trade-wind regions and in the extra-tropics, where one could expect the two types of clouds to co-exist. However, they represent a small part of the total low-cloud fraction (Fig. 14, fourth row). Finally, the ratio of Sc clouds to Sc and Cu clouds document the regions dominated by each type of clouds (Fig. 13, bottom row). Such information could be very useful to evaluate GCMs, which struggle to reproduce the Sc and Cu transition (e.g., Teixeira et al., 2011). The CASCCAD products robustly describe tropical oceans being almost exclusively dominated by Cu clouds while the western coasts of the continents are mostly covered by Sc clouds. Such picture is consistent with previous results from field campaigns, e.g., along the Global Energy and Water Experiment (GEWEX) Cloud System Studies (GCSS) Pacific Cross-Section Intercomparison (GPCI) transect (e.g., Zhou et al., 2015), or ship-based observations in the southeastern Pacific (Garay et al., 2008) and ground-based data, e.g., over the

Barbados (e.g., Nuijens et al., 2015). Finally, the CASCCAD products classify less Sc than the other products (Fig. 13 and 14, second row) in the extra-tropics and polar regions (poleward of 35˚), where the cloud feedbacks due to a change in low-cloud cover is somewhat less important –yet non-negligible– than in the tropics (Zelinka et al., 2016). Unsurprisingly, the transitioning Sc-Cu cloud fraction is also the largest in the extratropics where both types have a similar and substantial cloud fraction (30 to 40 %).

In all the passive satellite products but MISR, most of the globe is dominated by Sc clouds, with higher frequency of large ratio (> 50%, Fig. 14, bottom row) as opposed to a more continuous distribution in the CASCCAD products and MISR. The passive-sensor results suggest that the optical thickness does not permit a clear distinction between Cu and Sc clouds, in agreement with earlier studies (e.g., Pincus et al., 1999), although clustering analysis from passive-sensor observations may represent a better alternative (Tselioudis et al., 2013, their Fig. 3). To further investigate this statement, we classify GOCCP low clouds as a function of their opacity. The low-cloud containing profiles that are diagnosed as opaque (i.e., no surface echo retrieved) have an optical thickness larger than approximately 3 (Guzman et al., 2017). This optical thickness is further used as a threshold to separate Sc (opaque clouds with COT > 3) from Cu clouds (thin clouds with COT < 3), which is about the same optical thickness used in the passive sensor (i.e, COT = 3.6) to distinguish Cu and Sc clouds (i.e., COT = 3.6). As for the passive-sensor satellite observations, this method does not allow a clear separation between the two cloud populations (Fig. S4) although the ratio of Sc to Sc and Cu of derived from the two methods are well-correlated (~ 0.65). However, it confirms that trade-wind regions have smaller opacity and therefore have a different radiative impact on surface and TOA fluxes than more opaque Sc-dominated regions.

4.2.2 Profiles

Figure 15 shows global zonal profiles of cloud fraction for Cu, Sc, transitioning and all low-level clouds as observed by GOCCP, RL-GeoProf and 2BCCL, for the first time. Consistent with the case studies and map analysis, 2BCCL observations retrieve clouds in the low-levels more frequently than GOCCP and RL-GeoProf (Fig. 15, top row) although the difference with RL-GeoProf is rather small compared to that with GOCCP (approximately two times larger). The large difference between GOCCP and RL-GeoProf cloud fractions in the low levels mostly comes from mid and high-level topped clouds (e.g., frontal clouds in the extra-tropics and cumulonimbus and congestus clouds in the tropics, Fig. S5), which typically obscure CALIPSO vision by attenuating the lidar beam before it reaches the low levels. When separated into cloud types, GOCCP and RL-GeoProf observations agree quite well for Sc and transitioning clouds globally and for Cu clouds in the deep tropics (15˚S/N) and down to 2 km in the subtropics and the extra-tropics (Fig. 15, 2nd row). Between 2 km and 1 km, RL-GeoProf diagnoses more Cu than GOCCP. Such a difference is due to the different sensitivities of the lidar and radar instruments to clouds. The lidar signal becomes quickly attenuated by the optically and geometrically thick Cu –besides the attenuation from overlapping mid or high-clouds– whereas CloudSat radar continues detecting clouds down to 1 km. Below 1 km the surface clutter and the lidar attenuation make it difficult to retrieve a reliable cloud fraction.

Earth Syst. Sci. Data Discuss., https://doi.org/10.5194/essd-2019-73
Manuscript under review for journal Earth Syst. Sci. Data
Discussion started: 22 May 2019

Consistent with the case study and geographical analysis (Section 4.2.1), the 2BCCL product diagnoses far more (less) Sc (Cu) than the CASCCAD products, making the ratio of Sc to Sc-and-Cu clouds largely dominated by Sc (Fig. 15, bottom row). Furthermore, the vertical distribution of Sc and Cu clouds substantially differs from that of the CASCCAD products. 2BCCL Sc clouds may extend up to 3 km while the most part of Cu clouds are concentrated around 1 km and almost exclusively in the tropics. This lack of Cu and excess of Sc clouds above 1 km in tropical subsidence regimes (Fig. 15, right column) is in disagreement the CASCCAD products but also with previous studies focused on Sc regions (Cesana et al., 2019a, their Fig. 6) and Cu regions (Nuijens et al., 2015a, their Fig. 2, see also Fig. S1)(Nuijens et al., 2015a)(Nuijens et al., 2015a). Therefore, one may think that 2BCCL overestimates (underestimates) Sc (Cu) clouds by mis-diagnosing some Cu clouds into Sc clouds. On the contrary, the CASCCAD products better match typical profiles of Sc and Cu clouds.

Finally, these global scale profiles are consistent with the physical processes controlling each type of clouds and measurements from previous literature. The Sc clouds –driven by radiative cooling– cap the PBL, a little higher than 1 km in the tropics and lower toward the poles, and their geometrical thickness is smaller than 1 km. Averaged over the tropical subsidence regimes (and in the extra-tropics, Fig. S6), the Sc vertical cloud fraction peaks between 9 and 12 %, depending on the dataset, whereas it is larger for Sc deck areas only (not shown). On the contrary, Cu cloud base –forced by surface fluxes– mostly form below 1 km, near the LCL, and vertically extend further aloft (around 2.5 km). Although the Cu map cloud fraction is smaller than that of Sc in the tropics (Fig. 13, compare the second and third rows), their vertical cloud fraction is about the same, between 8 and 10 %, because they cover a larger domain (Fig. 15, right column). While the Sc vertical cloud fraction remains unchanged in the extra-tropics, its Cu counterpart appears slightly larger, up to 15 % for RL-GeoProf (Fig. S6).

5 Conclusion

In this paper, we document spatial distributions and profiles of stratocumulus (Sc) and cumulus (Cu) clouds on a global scale. To this end, we design a discrimination algorithm (DA; Section 3) that distinguishes Sc and Cu based on three observable cloud-properties: cloud top height (CTH), horizontal cloud fraction (HCF) and vertical cloud fraction variability (VCF). These simple criteria are sufficient to characterize the distinctive shape of Cu, which have a limited horizontal extent and highly variable CTH as opposed to Sc, which cover larger areas and have a small and stable geometrical thickness. The DA is utilized on instantaneous profiles of active-sensor CALIPSO-GOCCP (Guzman et al., 2017) and CloudSat-CALIPSO combined observations (RL-GeoProf; Cesana et al., 2019b; Mace and Zhang, 2014) to create the Cumulus And Stratocumulus CloudSat-CAlipso Datasets (CASCCAD) .

The choice of DA parameters is then investigated in Cu, Sc and Sc-Cu transitioning case studies (Section 4.1), supported by additional viewings from MODIS true reflectance and full resolution CALIPSO VFM ($\Delta z = 30$m). The results show that the DA robustly captures Sc, Cu and Sc-Cu transitioning clouds although the choice of VCF and HCF thresholds may slightly affect the Sc-Cu partitioning in open-Sc and Cu regions.

The CASCCAD global-scale statistics (Section 4.2) are then compared to a subset of passive-sensor satellite datasets and to the only existing CloudSat-CALIPSO cloud-type climatology 2B-CLDCLASS-LIDAR (2BCCL, Sassen and Wang, 2008). In passive-sensor satellite observations, which distinguish Sc and Cu only based on their cloud optical thickness, Sc and Cu co-exist everywhere and no region is fully dominated by a particular type of cloud (Fig. 12, bottom row). On the contrary, Sc clouds largely dominate the global statistics from the 2BCCL point of view, which may mis-diagnose a substantial portion of Cu clouds as Sc clouds in the trade-wind and extra-tropical regions. Interestingly, the CASCCAD observations depict tropical oceans being almost exclusively dominated by Cu clouds (20 to 40 %) while the oceans off the west coasts of the continents are mostly covered by Sc clouds (50 to 85 %), with transitioning clouds in between (10 to 15 %). Our results provide a broader context to earlier findings from ground-based and field campaigns (Albrecht et al., 2019, 1995; Bretherton et al., 2010; Comstock et al., 2004; Garay et al., 2008; Wood, 2012; Zhou et al., 2015; Zuidema et al., 2009). For example, our globally-averaged profiles of Cu cloud fraction over the tropical oceans are almost identical to that found by Nuijens et al. (2015a) over the Barbados, in terms of shape (cloud base below 1 km and cloud top above 2 km) and frequency of occurrence (~ 10 %). Another interesting result concerns the distribution and magnitude of Sc cloud fraction. Our results indicate that the Sc clouds occur up to 85 % of the time over Sc deck areas compared to 60 % in earlier studies (i.e., Wood, 2012) and that their presence in trade-wind regions is negligible as opposed to a 20 % cloud frequency (i.e., Wood, 2012). Furthermore, our analysis indicates that the optical thickness, albeit useful, is not a sufficient parameter to discriminate Cu from Sc clouds, in agreement with previous literature (e.g., Pincus et al., 1999).

Finally, by documenting the global geographical distribution of Sc and Cu clouds for the first time, the CASCCAD datasets make it possible to evaluate the shallow convection (Cu type) and boundary layer (Sc type) clouds in state-of-the art climate models, which are typically generated by distinct parametrizations (i.e., Cesana et al., 2019a). By doing so, one could also assess the radiative contribution of Sc and Cu clouds to climate and potentially improve our understanding of low-level cloud feedbacks.

Data availability

The CASCCAD statistical datasets (Cesana, 2019) can be downloaded on the GISS website (https://data.giss.nasa.gov/clouds/casccad/) and on the zenodo website (https://zenodo.org/record/2667637; DOI: http://doi.org/10.5281/zenodo.2667637).

GOCCP instantaneous profiles used to produce the CASCCAD dataset were downloaded from the CFMIP-Obs website (http://climserv.ipsl.polytechnique.fr/cfmip-obs/Calipso_goccp.html). The CloudSat–CALIPSO data used to produce the CASCCAD dataset (i.e., 2B-GEOPROF and 2B-GEOPROF-LIDAR) and the 2B-CLDCLASS-LIDAR product were obtained from the CloudSat Data Processing Center (http://www.cloudsat.cira.colostate.edu/data-products/level-2b).

Earth Syst. Sci. Data Discuss., https://doi.org/10.5194/essd-2019-73
Manuscript under review for journal Earth Syst. Sci. Data
Discussion started: 22 May 2019

Author contributions

GC designed the study, developed the products and carried out the analysis with inputs from AD and HC. GC wrote the manuscript with contributions from AD and HC.

Competing interests

The authors declare that they have no conflict of interest.

Acknowledgements

GC and AD were supported by a CloudSat-CALIPSO RTOP at the NASA Goddard Institute for Space Studies. The authors would like to thank NASA and CNES for giving access to CALIPSO and CloudSat observations, and Climserv for giving access to CALIPSO-GOCCP observations and for providing computing resources. GC thanks Zhien Wang for his help in understanding the 2B-CLDCLASS-LIDAR dataset and Andy Ackerman, Ann Fridlind, Max Kelley and Greg Elsaesser for helpful comments and discussion.

References

Albrecht, B., Ghate, V., Mohrmann, J., Wood, R., Zuidema, P., Bretherton, C., Schwartz, C., Eloranta, E., Glienke, S., Donaher, S., Sarkar, M., McGibbon, J., Nugent, A. D., Shaw, R. A., Fugal, J., Minnis, P., Paliknoda, R., Lussier, L., Jensen, J., Vivekanandan, J., Ellis, S., Tsai, P., Rilling, R., Haggerty, J., Campos, T., Stell, M., Reeves, M., Beaton, S., Allison, J., Stossmeister, G., Hall, S. and Schmidt, S.: Cloud system evolution in the trades (CSET)following the evolution of boundary layer cloud systems with the NSF-NCAR GV, Bull. Am. Meteorol. Soc., 100(1), 93–121, doi:10.1175/BAMS-D-17-0180.1, 2019.

Albrecht, B. A., Bretherton, C. S., Johnson, D., Scubert, W. H. and Frisch, A. S.: The Atlantic Stratocumulus Transition Experiment—ASTEX, Bull. Am. Meteorol. Soc., 76(6), 889–904, doi:10.1175/1520-0477(1995)076<0889:TASTE>2.0.CO;2, 1995.

Bretherton, C. S.: Insights into low-latitude cloud feedbacks from high-resolution models, Philos. Trans. R. Soc. A Math. Phys. Eng. Sci., 373(2054), doi:10.1098/rsta.2014.0415, 2015.

Bretherton, C. S., Wood, R., George, R. C., Leon, D., Allen, G. and Zheng, X.: Southeast Pacific stratocumulus clouds, precipitation and boundary layer structure sampled along 20° S during VOCALS-REx, Atmos. Chem. Phys., 10(21), 10639–10654, doi:10.5194/acp-10-10639-2010, 2010.

Cesana, G.: CASCCAD: Cumulus And Stratocumulus Cloudsat-CAlipso Dataset [Data set], Zenodo. http://doi.org/10.5281/zenodo.2667637, 2019.

Cesana, G. and Waliser, D. E.: Characterizing and understanding systematic biases in the vertical structure of clouds in CMIP5/CFMIP2 models, Geophys. Res. Lett., 43(19), 10,538-10,546, doi:10.1002/2016GL070515, 2016.

Cesana, G., Chepfer, H., Winker, D., Getzewich, B., Cai, X., Jourdan, O., Mioche, G., Okamoto, H., Hagihara, Y., Noel, V. and Reverdy, M.: Using in situ airborne measurements to evaluate three cloud phase products derived from CALIPSO, J. Geophys. Res., 121(10), 5788–5808, doi:10.1002/2015JD024334, 2016.

Cesana, G., Del Genio, A. D., Ackerman, A. S., Kelley, M., Elsaesser, G., Fridlind, A. M., Cheng, Y. and Yao, M.-S.: Evaluating models' response of tropical low clouds to SST forcings using CALIPSO observations, Atmos. Chem. Phys., 19(5), 2813–2832, doi:10.5194/acp-19-2813-2019, 2019a.

Cesana, G., Waliser, D. E., Henderson, D., L'Ecuyer, T. S., Jiang, X. and Li, J.-L. F.: The Vertical Structure of Radiative Heating Rates: A Multimodel Evaluation Using A-Train Satellite Observations, J. Clim., 32(5), 1573–1590, doi:10.1175/JCLI-D-17-0136.1, 2019b.

Chepfer, H., Bony, S., Winker, D., Chiriaco, M., Dufresne, J. and Se, G.: Use of CALIPSO lidar observations to evaluate the cloudiness simulated by a climate model, , 35, 1–6, doi:10.1029/2008GL034207, 2008.

Chepfer, H., Bony, S., Winker, D., Cesana, G., Dufresne, J. L., Minnis, P., Stubenrauch, C. J. and Zeng, S.: The GCM-Oriented CALIPSO Cloud Product (CALIPSO-GOCCP), J. Geophys. Res., 115(5), D00H16, doi:10.1029/2009JD012251, 2010.

Chepfer, H., Cesana, G., Winker, D., Getzewich, B., Vaughan, M. and Liu, Z.: Comparison of Two Different Cloud Climatologies Derived from CALIOP-Attenuated Backscattered Measurements (Level 1): The CALIPSO -ST and the CALIPSO -GOCCP, J. Atmos. Ocean. Technol., 30(4), 725–744, doi:10.1175/JTECH-D-12-00057.1, 2013.

Comstock, K. K., Wood, R., Yuter, S. E. and Bretherton, C. S.: Reflectivity and rain rate in and below drizzling stratocumulus, Q. J. R. Meteorol. Soc., 130(603), 2891–2918, doi:10.1256/qj.03.187, 2004.

Garay, M. J., Szoeke, S. P. De and Moroney, C. M.: Comparison of marine stratocumulus cloud top heights in the southeastern Pacific retrieved from satellites with coincident ship-based observations, , 113, 1–13, doi:10.1029/2008JD009975, 2008.

Guzman, R., Chepfer, H., Noel, V., de Guélis, T. V., Kay, J. E., Raberanto, P., Cesana, G., Vaughan, M. A. and Winker, D. M.: Direct atmosphere opacity observations from CALIPSO provide new constraints on cloud-radiation interactions, J. Geophys. Res., 122(2), 1066–1085, doi:10.1002/2016JD025946, 2017.

Hahn, C. J. and Warren, S. G.: A GRIDDED CLIMATOLOGY OF CLOUDS, Analysis, doi:10.3334/CDIAC/cli.ndp026e, 2007.

Hahn, C. J., Rossow, W. B. and Warren, S. G.: ISCCP Cloud Properties Associated with Standard Cloud Types Identified in Individual Surface Observations, J. Clim., 14(1), 11–28, doi:10.1175/1520-0442(2001)014<0011:ICPAWS>2.0.CO;2, 2001.

Huang, L., Jiang, J. H., Wang, Z., Su, H., Deng, M. and Massie, S.: Climatology of cloud water content associated with different cloud types observed by A-Train satellites, J. Geophys. Res. Atmos., 120(9), 4196–4212, doi:10.1002/2014JD022779, 2015.

King, M. D., Platnick, S., Menzel, W. P., Ackerman, S. A. and Hubanks, P. A.: Spatial and Temporal Distribution of Clouds Observed by MODIS Onboard the Terra and Aqua Satellites, IEEE Trans. Geosci. Remote Sens., 51(7), 3826–3852, doi:10.1109/TGRS.2012.2227333, 2013.

Klein, S. A. and Hall, A.: Emergent Constraints for Cloud Feedbacks, Curr. Clim. Chang. Reports, 1(4), 276–287, doi:10.1007/s40641-015-0027-1, 2015.

Klein, S. A., Hall, A., Norris, J. R. and Pincus, R.: Low-Cloud Feedbacks from Cloud-Controlling Factors: A Review, Surv. Geophys., 38(6), 1307–1329, doi:10.1007/s10712-017-9433-3, 2017.

Lacour, A., Chepfer, H., Shupe, M. D., Miller, N. B., Noel, V., Kay, J., Turner, D. D. and Guzman, R.: Greenland Clouds Observed in CALIPSO -GOCCP: Comparison with Ground-Based Summit Observations, J. Clim., 30(15), 6065–6083, doi:10.1175/JCLI-D-16-0552.1, 2017.

Lamer, K., Kollias, P. and Nuijens, L.: Observations of the variability of shallow trade wind cumulus cloudiness and mass flux, J. Geophys. Res. Atmos., 120(12), 6161–6178, doi:10.1002/2014JD022950, 2015.

Mace, G. G. and Zhang, Q.: The CloudSat radar-lidar geometrical profile product (RL-GeoProf): Updates, improvements, and selected results, J. Geophys. Res. Atmos., 119(15), 9441–9462, doi:10.1002/2013JD021374, 2014.

Marchand, R., Haynes, J., Mace, G. G., Ackerman, T. and Stephens, G.: A comparison of simulated cloud radar output from the multiscale modeling framework global climate model with CloudSat cloud radar observations, J. Geophys. Res., 114(8), D00A20, doi:10.1029/2008JD009790, 2009.

Marchand, R., Ackerman, T., Smyth, M. and Rossow, W. B.: A review of cloud top height and optical depth histograms from MISR, ISCCP, and MODIS, J. Geophys. Res. Atmos., 115(16), 1–25, doi:10.1029/2009JD013422, 2010.

McCoy, D. T., Eastman, R., Hartmann, D. L. and Wood, R.: The change in low cloud cover in a warmed climate inferred from AIRS, MODIS, and ERA-interim, J. Clim., 30(10), 3609–3620, doi:10.1175/JCLI-D-15-0734.1, 2017.

Mcgill, M. J., Vaughan, M. A., Trepte, C. R., Hart, W. D., Hlavka, D. L., Winker, D. M. and Kuehn, R.: Airborne validation of spatial properties measured by the CALIPSO lidar, , 112, 1–8, doi:10.1029/2007JD008768, 2007.

Nuijens, L., Medeiros, B., Sandu, I. and Ahlgrimm, M.: Observed and modeled patterns of covariability between low-level cloudiness and the structure of the trade-wind layer, J. Adv. Model. Earth Syst., 7(4), 1741–1764, doi:10.1002/2015MS000483, 2015a.

Nuijens, L., Medeiros, B., Sandu, I. and Ahlgrimm, M.: The behavior of trade-wind cloudiness in observations and models: The major cloud components and their variability, J. Adv. Model. Earth Syst., 7(2), 600–616, doi:10.1002/2014MS000390, 2015b.

Pincus, R., McFarlane, S. A. and Klein, S. A.: Albedo bias and the horizontal variability of clouds in subtropical marine boundary layers: Observations from ships and satellites, J. Geophys. Res. Atmos., 104(D6), 6183–6191, doi:10.1029/1998JD200125, 1999.

Rauber, R. M., Stevens, B., Ochs, H. T., Knight, C., Albrecht, B. a., Blyth, a. M., Fairall, C. W. and Jensen, J. B.: Over the ocean: The RICO campaign, Bull. Am. Meteorol. Soc., (December 2007), 1912–1928, doi:10.1175/BAMS-88-12-1912, 2007.

Rodts, S. M. A., Duynkerke, P. G. and Jonker, H. J. J.: Size Distributions and Dynamical Properties of Shallow Cumulus Clouds from Aircraft Observations and Satellite Data, J. Atmos. Sci., 60(16), 1895–1912, doi:10.1175/1520-0469(2003)060<1895:SDADPO>2.0.CO;2, 2003.

Rossow, W. B. and Schiffer, R. A.: ISCCP Cloud Data Products, Bull. Am. Meteorol. Soc., 72(1), 2–20, doi:10.1175/1520-0477(1991)072<0002:ICDP>2.0.CO;2, 1991.

Rossow, W. B. and Schiffer, R. A.: Advances in Understanding Clouds from ISCCP, Bull. Am. Meteorol. Soc., 80(11), 2261–2287, doi:10.1175/1520-0477(1999)080<2261:AIUCFI>2.0.CO;2, 1999.

Sassen, K. and Wang, Z.: Classifying clouds around the globe with the CloudSat radar : 1-year of results, , 35(January), 1–5, doi:10.1029/2007GL032591, 2008.

Stephens, G. L., Vane, D. G., Boain, R. J., Mace, G. G., Sassen, K., Wang, Z., Illingworth, A. J., O'connor, E. J., Rossow, W. B., Durden, S. L., Miller, S. D., Austin, R. T., Benedetti, A. and Mitrescu, C.: THE CLOUDSAT MISSION AND THE A-TRAIN, Bull. Am. Meteorol. Soc., 83(12), 1771–1790, doi:10.1175/BAMS-83-12-1771, 2002.

Takahashi, N., Oki, R., Kikuchi, M., Cesana, G., Hayasaka, T., Sato, K., Hagihara, Y., Okamoto, H. and Suzuki, K.: Development of Algorithm for Discriminating Hydrometeor Particle Types With a Synergistic Use of CloudSat and CALIPSO, J. Geophys. Res. Atmos., 122(20), 11,022-11,044, doi:10.1002/2017jd027113, 2017.

Teixeira, J., Cardoso, S., Bonazzola, M., Cole, J., DelGenio, A., DeMott, C., Franklin, C., Hannay, C., Jakob, C., Jiao, Y., Karlsson, J., Kitagawa, H., Köhler, M., Kuwano-Yoshida, A., LeDrian, C., Li, J., Lock, A., Miller, M. J., Marquet, P., Martins, J., Mechoso, C. R., Meijgaard, E. v., Meinke, I., Miranda, P. M. A., Mironov, D., Neggers, R., Pan, H. L., Randall, D. A., Rasch, P. J., Rockel, B., Rossow, W. B., Ritter, B., Siebesma, A. P., Soares, P. M. M., Turk, F. J., Vaillancourt, P. A., Von Engeln, A. and Zhao, M.: Tropical and Subtropical Cloud Transitions in Weather and Climate Prediction Models: The GCSS/WGNE Pacific Cross-Section Intercomparison (GPCI), J. Clim., 24(20), 5223–5256, doi:10.1175/2011JCLI3672.1, 2011.

Thorsen, T. J., Fu, Q. and Comstock, J. M.: Cloud effects on radiative heating rate profiles over Darwin using ARM and A-train radar/lidar observations, J. Geophys. Res. Atmos., 118(11), 5637–5654, doi:10.1002/jgrd.50476, 2013.

Tselioudis, G., Rossow, W., Zhang, Y. and Konsta, D.: Global weather states and their properties from passive and active satellite cloud retrievals, J. Clim., 26(19), 7734–7746, doi:10.1175/JCLI-D-13-00024.1, 2013.

Vaughan, M. A., Powell, K. A., Winker, D. M., Hostetler, C. A., Kuehn, R. E., Hunt, W. H., Getzewich, B. J., Young, S. A., Liu, Z. and McGill, M. J.: Fully Automated Detection of Cloud and Aerosol Layers in the CALIPSO Lidar Measurements, J. Atmos. Ocean. Technol., 26(10), 2034–2050, doi:10.1175/2009JTECHA1228.1, 2009.

Wang, Z., Vane, D., Stephens, G. and Reinke, D.: Level 2 Combined Radar and Lidar Cloud Scenario Classification Product Process Description and Interface Control document, CloudSat Proj. Jet Propuls. Lab. Pasadena …, (D), 2013.

Winker, D. M., Pelon, J., Coakley, J. A., Ackerman, S. A., Charlson, R. J., Colarco, P. R., Flamant, P., Fu, Q., Hoff, R. M., Kittaka, C., Kubar, T. L., Le Treut, H., Mccormick, M. P., Mégie, G., Poole, L., Powell, K., Trepte, C., Vaughan, M. A.

and Wielicki, B. A.: The CALIPSO Mission, Bull. Am. Meteorol. Soc., 91(9), 1211–1230, doi:10.1175/2010BAMS3009.1, 2010.

Wood, R.: Stratocumulus Clouds, Mon. Weather Rev., 140(8), 2373–2423, doi:10.1175/MWR-D-11-00121.1, 2012.

Wyant, M. C., Bretherton, C. S., Rand, H. A. and Stevens, D. E.: Numerical Simulations and a Conceptual Model of the Stratocumulus to Trade Cumulus Transition, J. Atmos. Sci., 54(1), 168–192, doi:10.1175/1520-0469(1997)054<0168:NSAACM>2.0.CO;2, 1997.

Zelinka, M. D., Zhou, C. and Klein, S. A.: Insights from a refined decomposition of cloud feedbacks, Geophys. Res. Lett., 43(17), 9259–9269, doi:10.1002/2016GL069917, 2016.

Zhang, Y. and Klein, S. A.: Factors Controlling the Vertical Extent of Fair-Weather Shallow Cumulus Clouds over Land: Investigation of Diurnal-Cycle Observations Collected at the ARM Southern Great Plains Site, J. Atmos. Sci., 70(4), 1297–1315, doi:10.1175/JAS-D-12-0131.1, 2013.

Zhou, X., Kollias, P. and Lewis, E. R.: Clouds, precipitation, and marine boundary layer structure during the MAGIC field campaign, J. Clim., 28(6), 2420–2442, doi:10.1175/JCLI-D-14-00320.1, 2015.

Zuidema, P., Painemal, D., De Szoeke, S. and Fairall, C.: Stratocumulus cloud-top height estimates and their climatic implications, J. Clim., 22(17), 4652–4666, doi:10.1175/2009JCLI2708.1, 2009.

Earth Syst. Sci. Data Discuss., https://doi.org/10.5194/essd-2019-73
Manuscript under review for journal Earth Syst. Sci. Data
Discussion started: 22 May 2019

Figures

Figure 1: Cartoon representing the different cloud morphologies used in this study. The blue dashed line denotes the upper limit of the low-level clouds following GOCCP definition (3.36 km). Note that the Deep Cu type is not a low cloud, but either a mid- or high-level cloud.

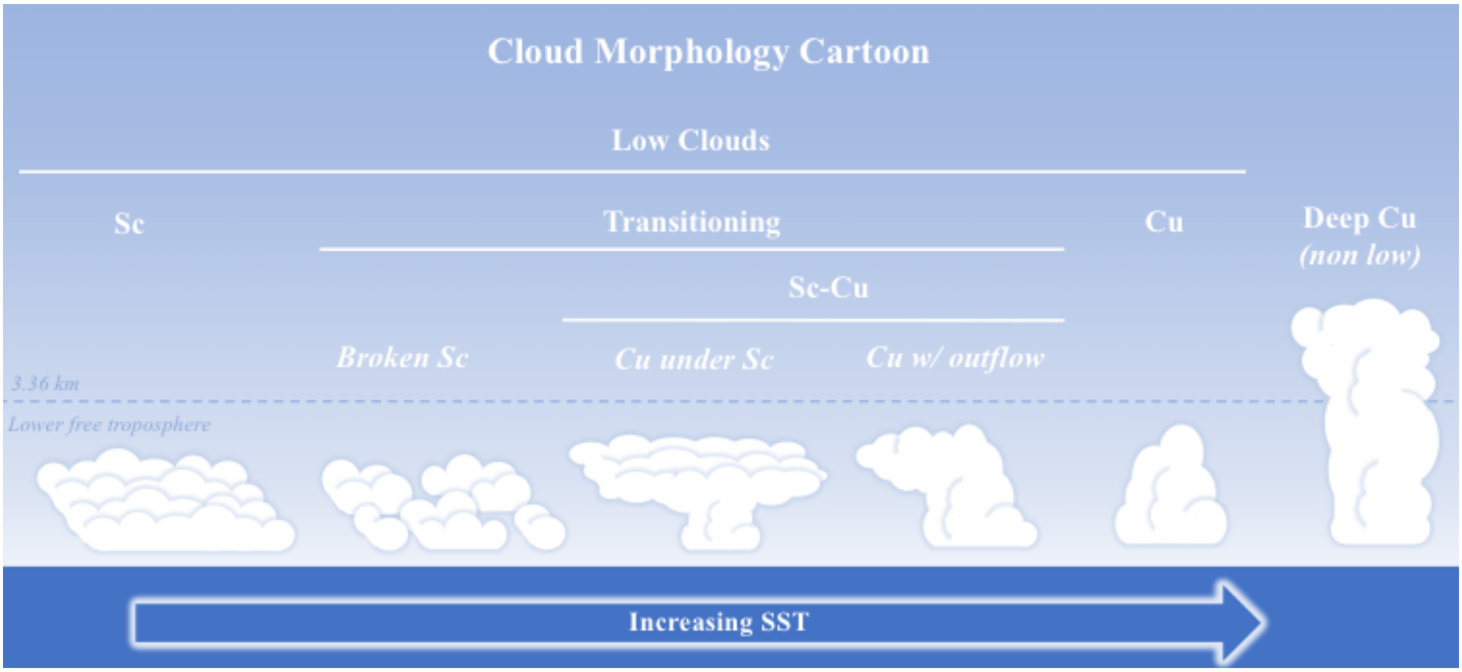

Figure 2: Flow diagram of the algorithm that performs the Sc-Cu discrimination. The grey, orange and purple colors represent the different steps of the discrimination algorithm to separate Sc, broken Sc, Cu and Sc-Cu transitioning clouds: height, horizontal extent and vertical extent, respectively. The choice of HCF thresholds is discussed in section 3.3 and theirs values are shown in Fig. 4. The VCF threshold (0.12) is also explained in section 3.4 and further used in Fig. 5.

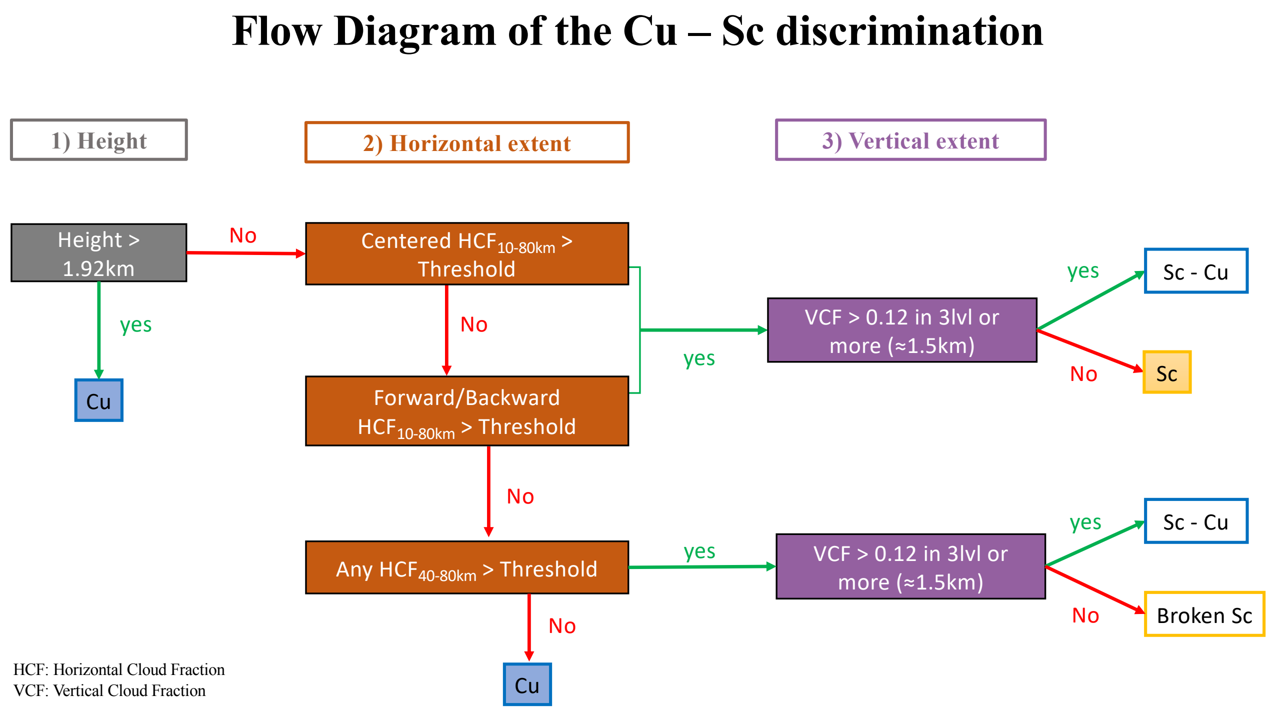

Figure 3: Cartoon of the horizontal along-track averaging that is used by the DA to compute the horizontal cloud fraction (HCF): a) the lidar beam is in the middle of the cloud and b) the lidar beam is at the edge of the cloud. The dark-green circles correspond to the profiles used to in the different horizontal averaging scenarios (centered, forward or backward).

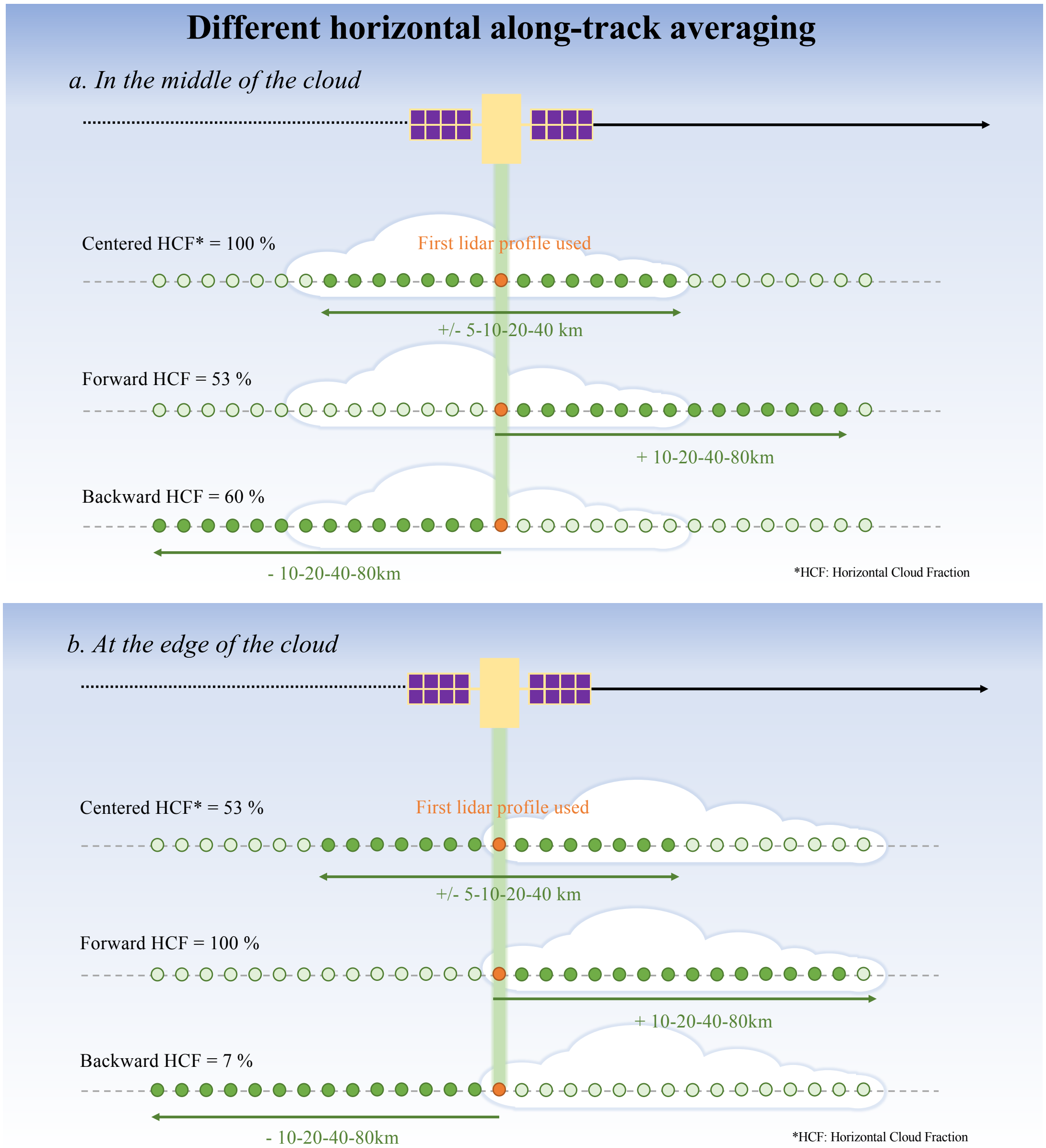

Earth Syst. Sci. Data Discuss., https://doi.org/10.5194/essd-2019-73
Manuscript under review for journal Earth Syst. Sci. Data
Discussion started: 22 May 2019

Figure 4: PDF of the different along-track CHCFs for Cu (blue) and Sc (light red) typical regions computed from eight orbit segments. The thresholds are represented in purple, at approximately the overlap of the two distributions.

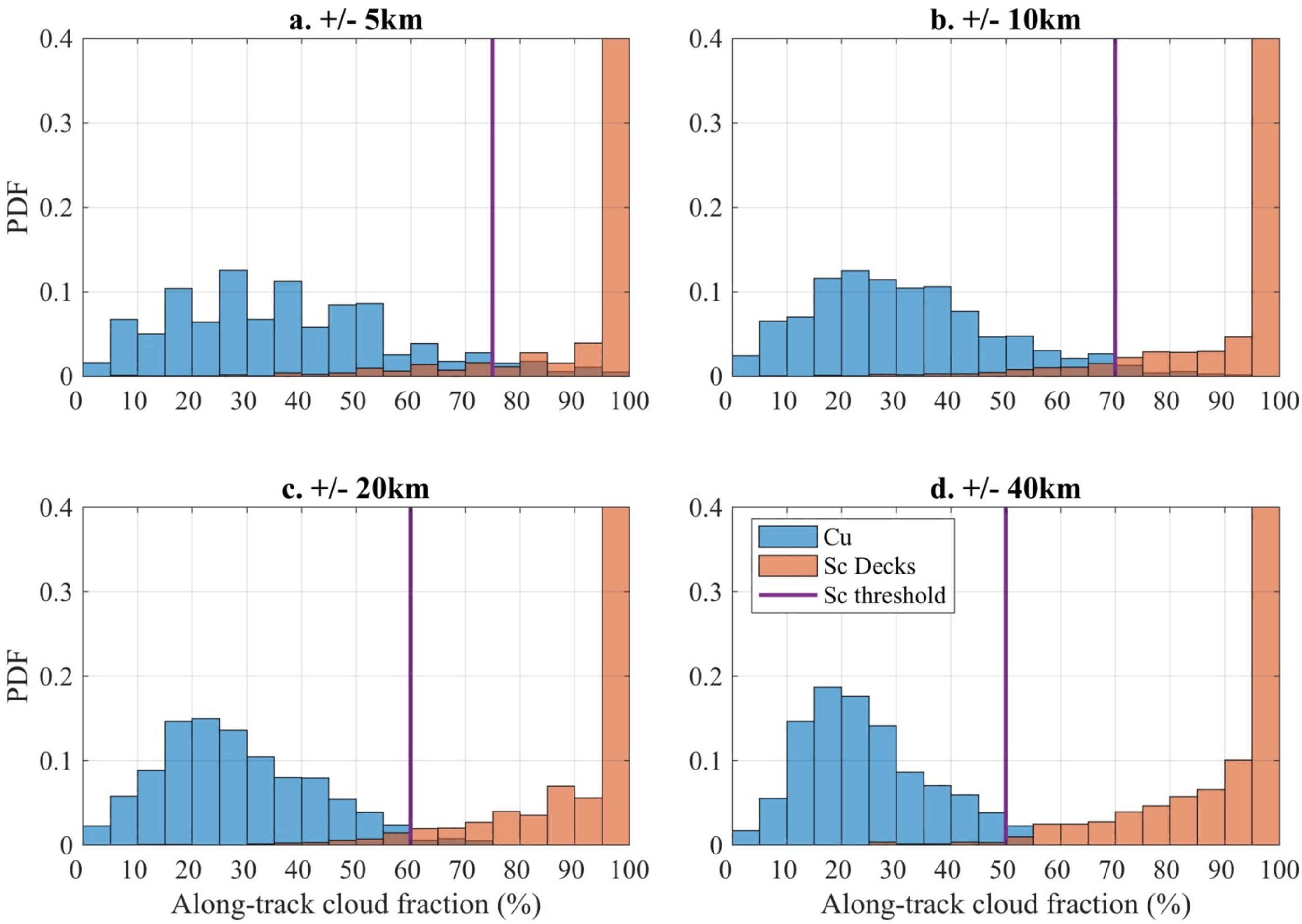

5

Earth Syst. Sci. Data Discuss., https://doi.org/10.5194/essd-2019-73
Manuscript under review for journal Earth Syst. Sci. Data
Discussion started: 22 May 2019

Figure 5: Cartoon of the additional diagnostics in the DA. After the DA diagnoses (a) an initial cloud type, the additional (b) "significant VCF variability" test and (c) "horizontal continuity" test are applied (See details in section 3.4 and 3.5).

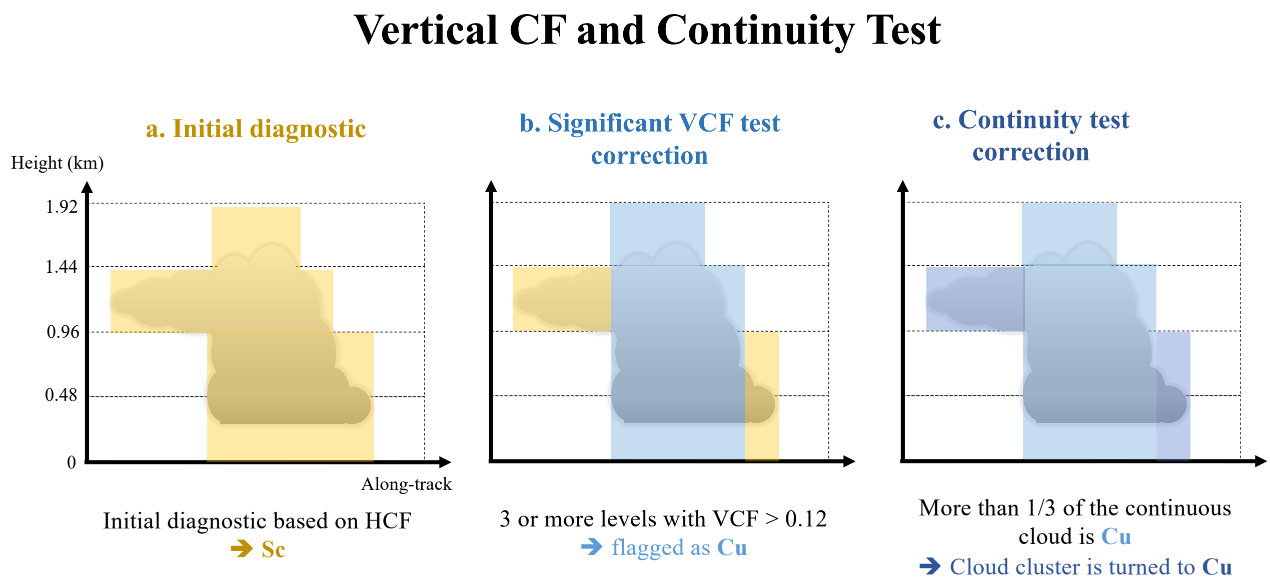

Earth Syst. Sci. Data Discuss., https://doi.org/10.5194/essd-2019-73
Manuscript under review for journal Earth Syst. Sci. Data
Discussion started: 22 May 2019

Figure 6: Daytime orbit segment off the coast of California (~ 8°N to 46°N, 2008-07-08 21:47:30) showing a typical stratocumulus case. (a) VFM CASLIPSO-ST at 30-m vertical resolution, (b) to (g) sensitivity of the GOCCP Sc-Cu mask to different DA parameters: (b) the VCF threshold is divided by 2, (c) the CTH threshold is elevated from 1.92 km to 2.4 km, (d) standard DA parameters, (e) the continuity test is turned off, (f) the 10-km and 20-km HCF thresholds are more conservative (i.e., increased by 0.1, absolute value) and (g) the 10-km and 20-km HCF thresholds are less conservative i.e., (decreased by 0.1, absolute value). The HCF of Sc (including broken Sc) and Cu (including Sc-Cu transitioning) are given in each subplot (top left corner). Reddish and bluish pixels correspond to Sc and Cu type of clouds, respectively. From the top to the bottom, the VFM color bar's labels correspond to undetermined, aerosol, cloudy, clear and fully attenuated pixels. From the top to the bottom, the GOCCP Sc-Cu mask color bar's labels correspond to cumulus, Sc-Cu transitioning, broken Sc, edge of Sc, stratocumulus, and clear pixels.

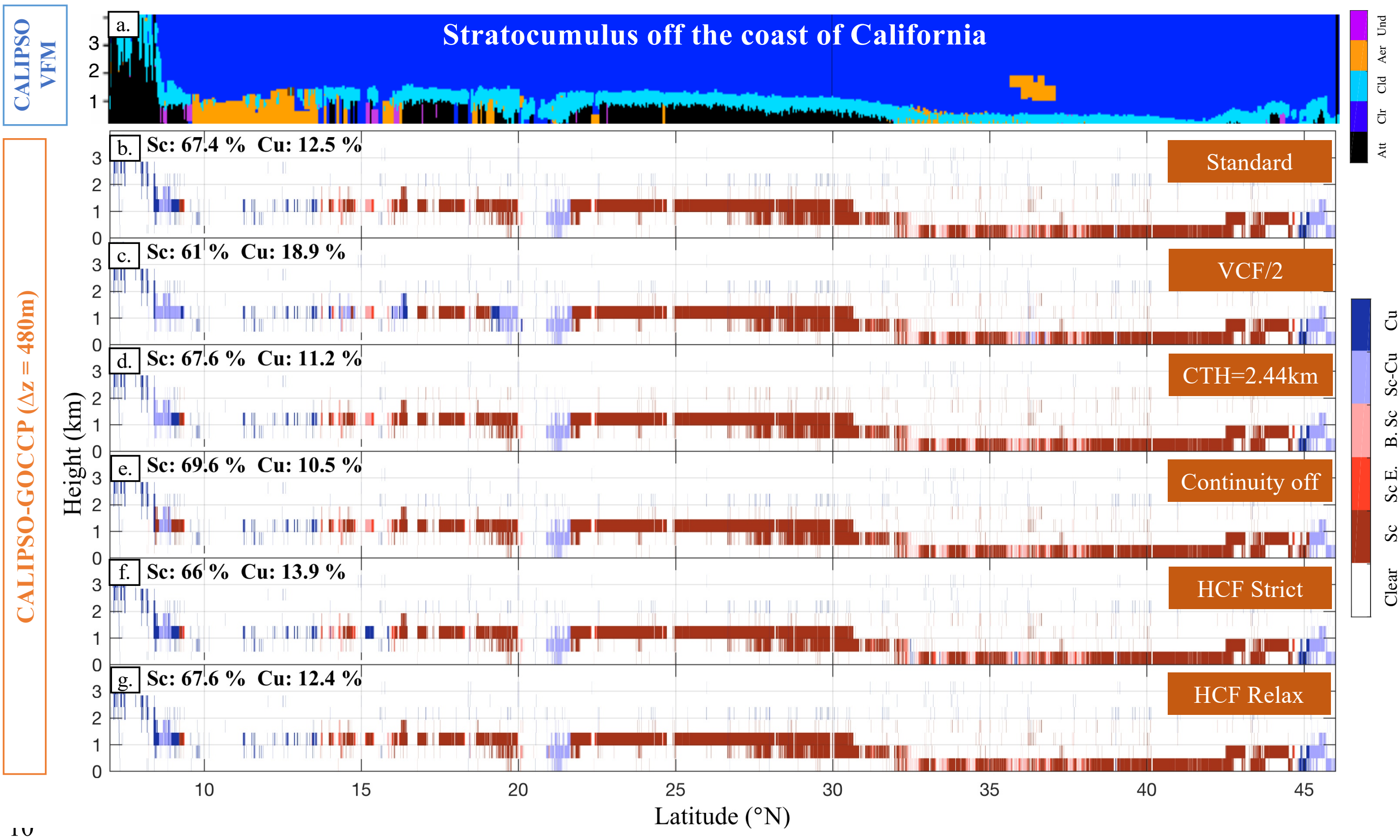

Earth Syst. Sci. Data Discuss., https://doi.org/10.5194/essd-2019-73
Manuscript under review for journal Earth Syst. Sci. Data
Discussion started: 22 May 2019

Figure 7: Same stratocumulus case study as in Fig. 5 but for (a) the standard GOCCP Sc-Cu mask (same as Fig. 5b), (b) the RL-GeoProf Sc-Cu mask, (c) 2BCCL cloud type mask and (d) MODIS true reflectance. The red line correspond to the CALIPSO-CloudSat overpass.

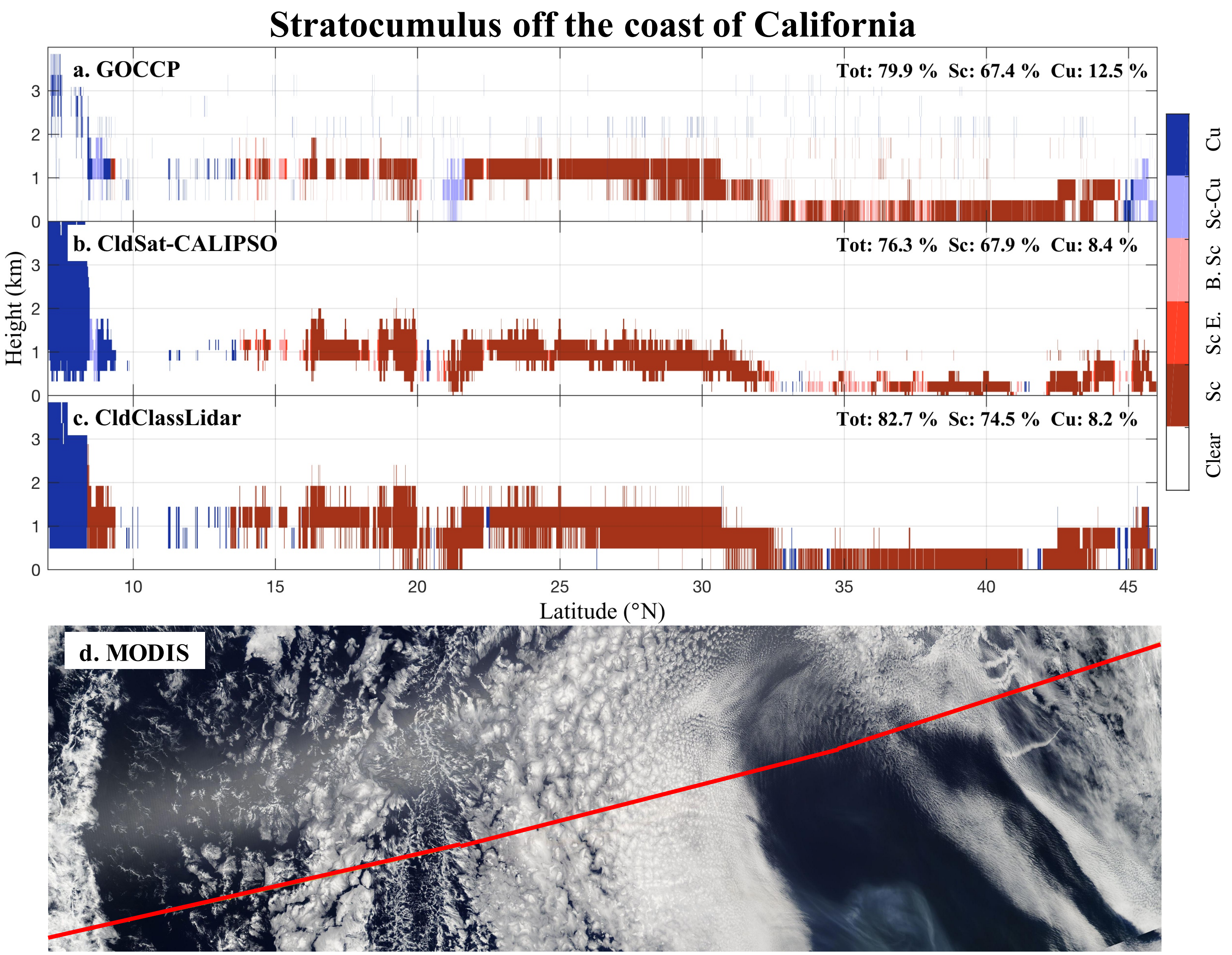

Earth Syst. Sci. Data Discuss., https://doi.org/10.5194/essd-2019-73
Manuscript under review for journal Earth Syst. Sci. Data
Discussion started: 22 May 2019

Figure 8: Same as Fig. 5 but for a typical cumulus case in the south-east Pacific (~ 37˚S to 8˚S, 2008-07-08 21:47:30, daytime).

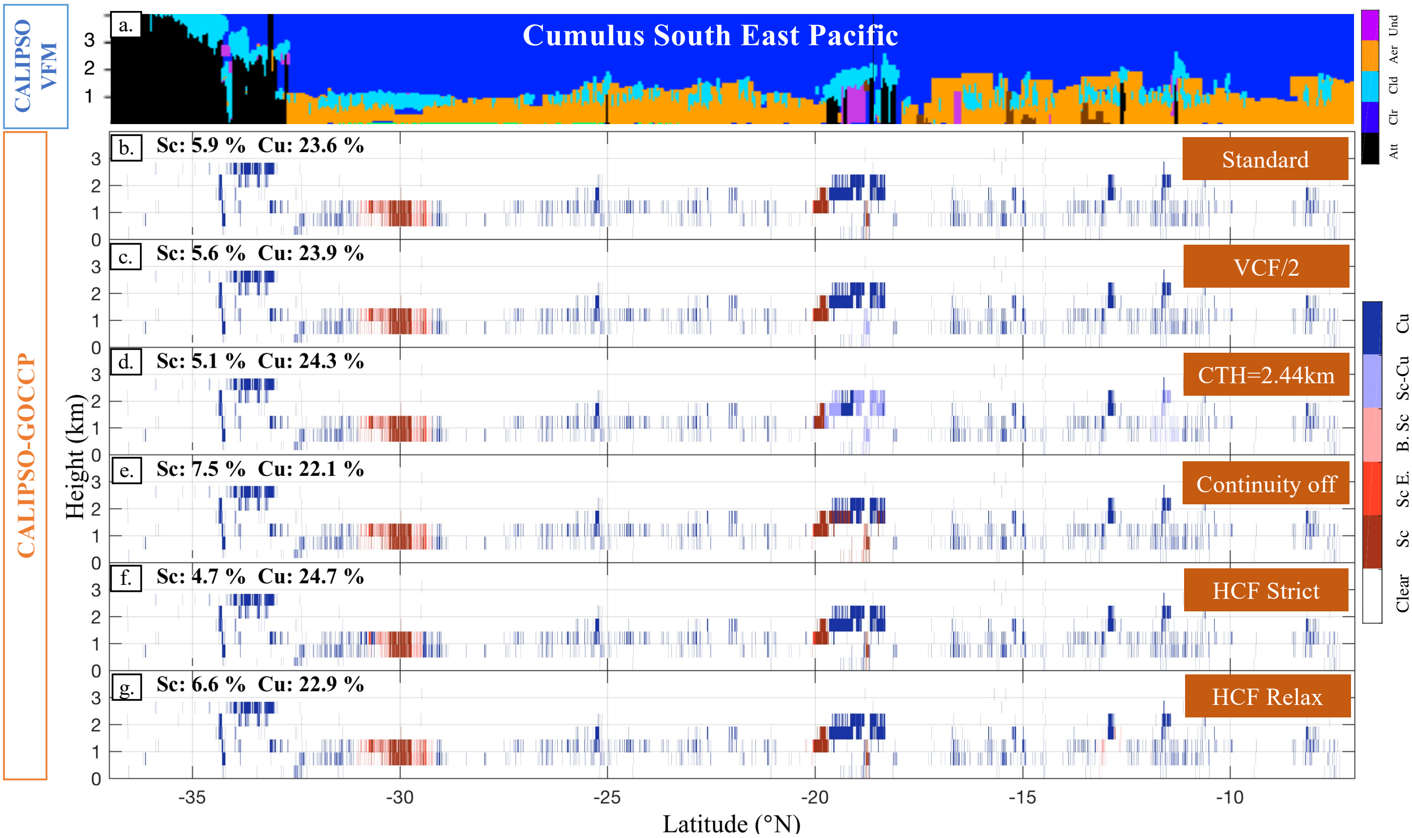

Earth Syst. Sci. Data Discuss., https://doi.org/10.5194/essd-2019-73
Manuscript under review for journal Earth Syst. Sci. Data
Discussion started: 22 May 2019

Open Access Earth System Science Data Discussions

Figure 9: Same as Fig. 6 but for a typical cumulus case in the south-east Pacific (~ 37˚S to 8˚S, 2008-07-08 21:47:30, daytime).

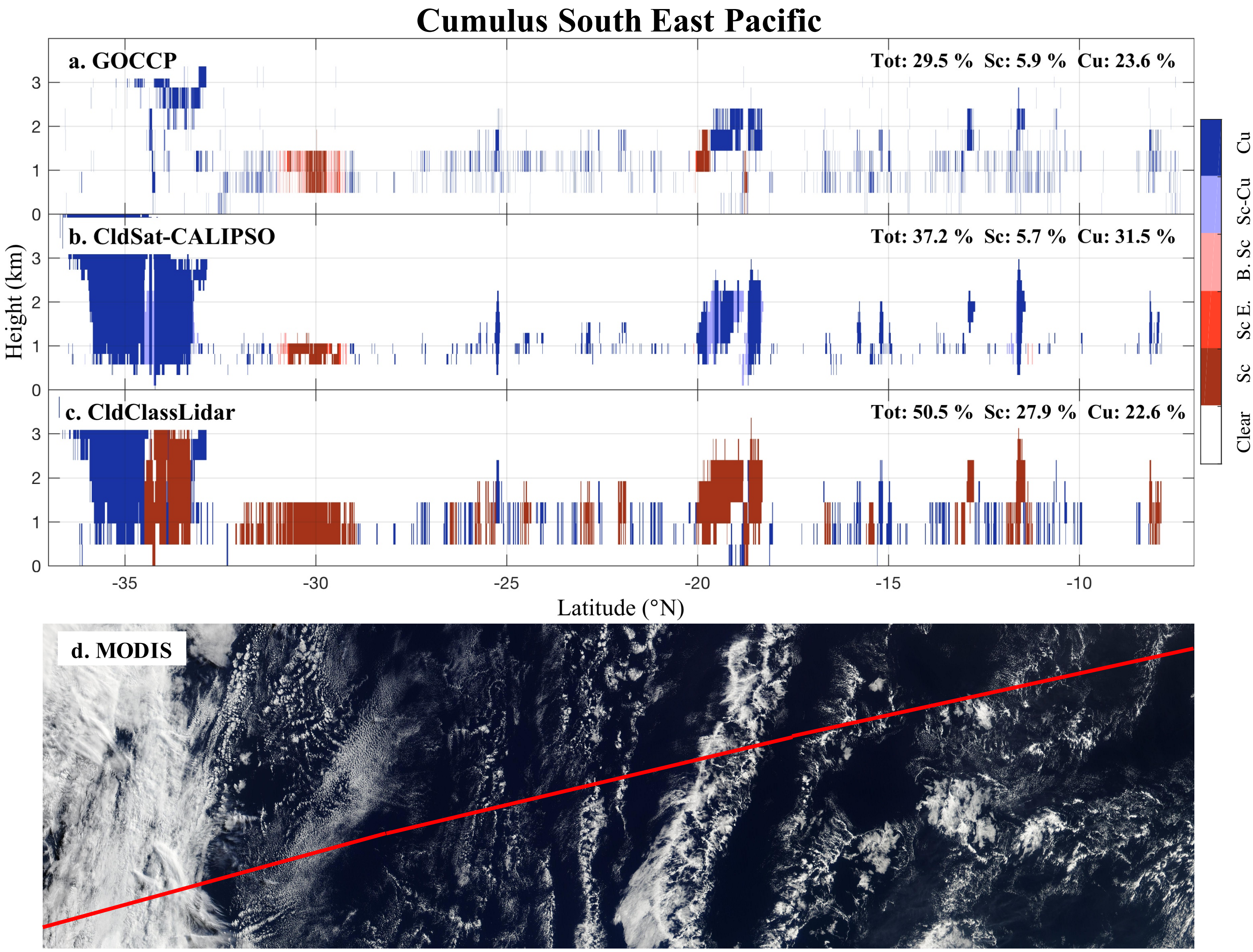

Earth Syst. Sci. Data Discuss., https://doi.org/10.5194/essd-2019-73
Manuscript under review for journal Earth Syst. Sci. Data
Discussion started: 22 May 2019

Figure 10: Same as Fig. 8 but for another cumulus case overpassing the Barbados (~ 10°N to 35°N, 2008-07-09 17:34:08 daytime)

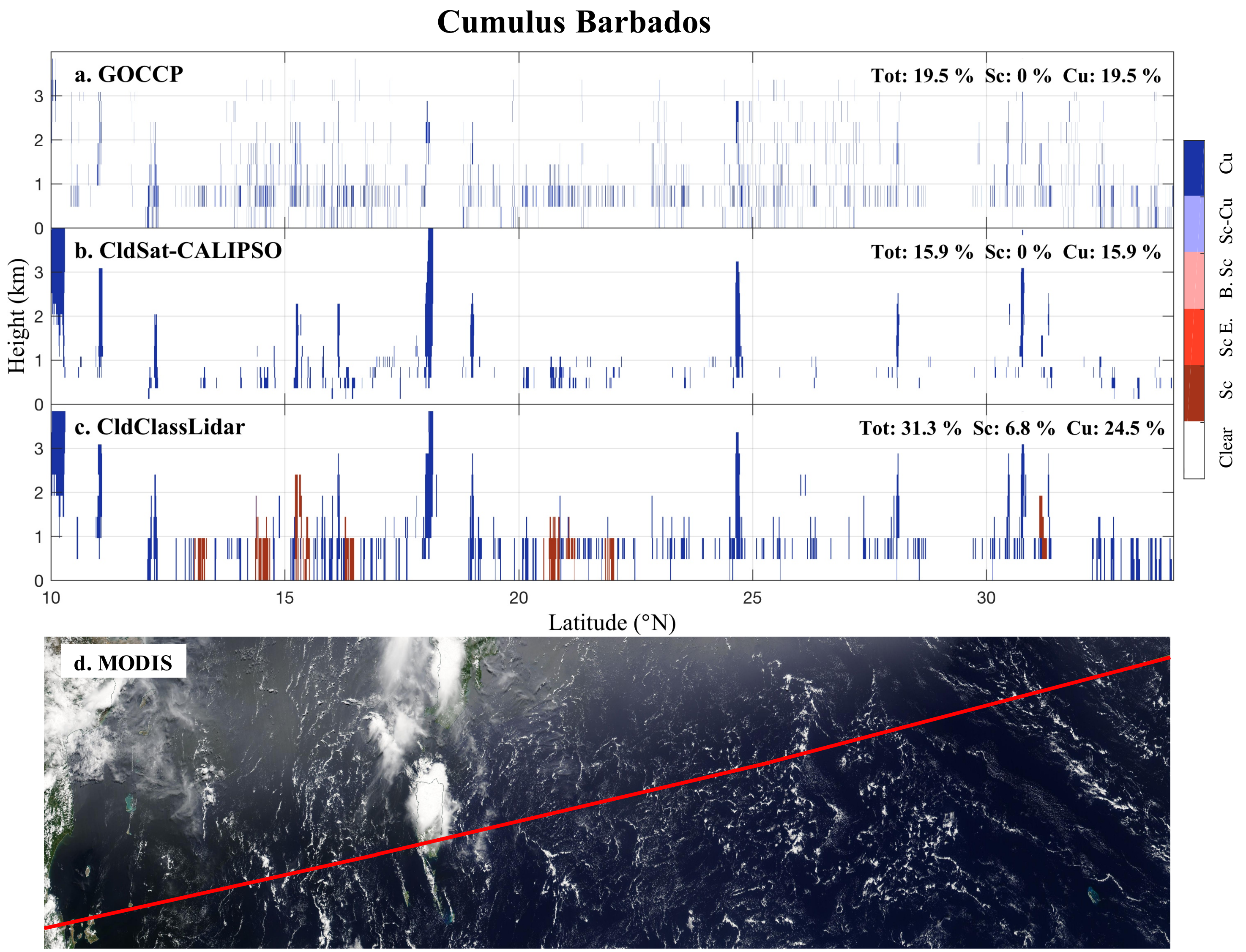

Earth Syst. Sci. Data Discuss., https://doi.org/10.5194/essd-2019-73
Manuscript under review for journal Earth Syst. Sci. Data
Discussion started: 22 May 2019

Figure 11: Same as Fig. 5 but for a typical Open-cell Sc to Cu transitioning case overlapping the south-east Pacific and the Southern Ocean (~ 55˚S to 20˚S, 2008-07-14 21:10:19, daytime).

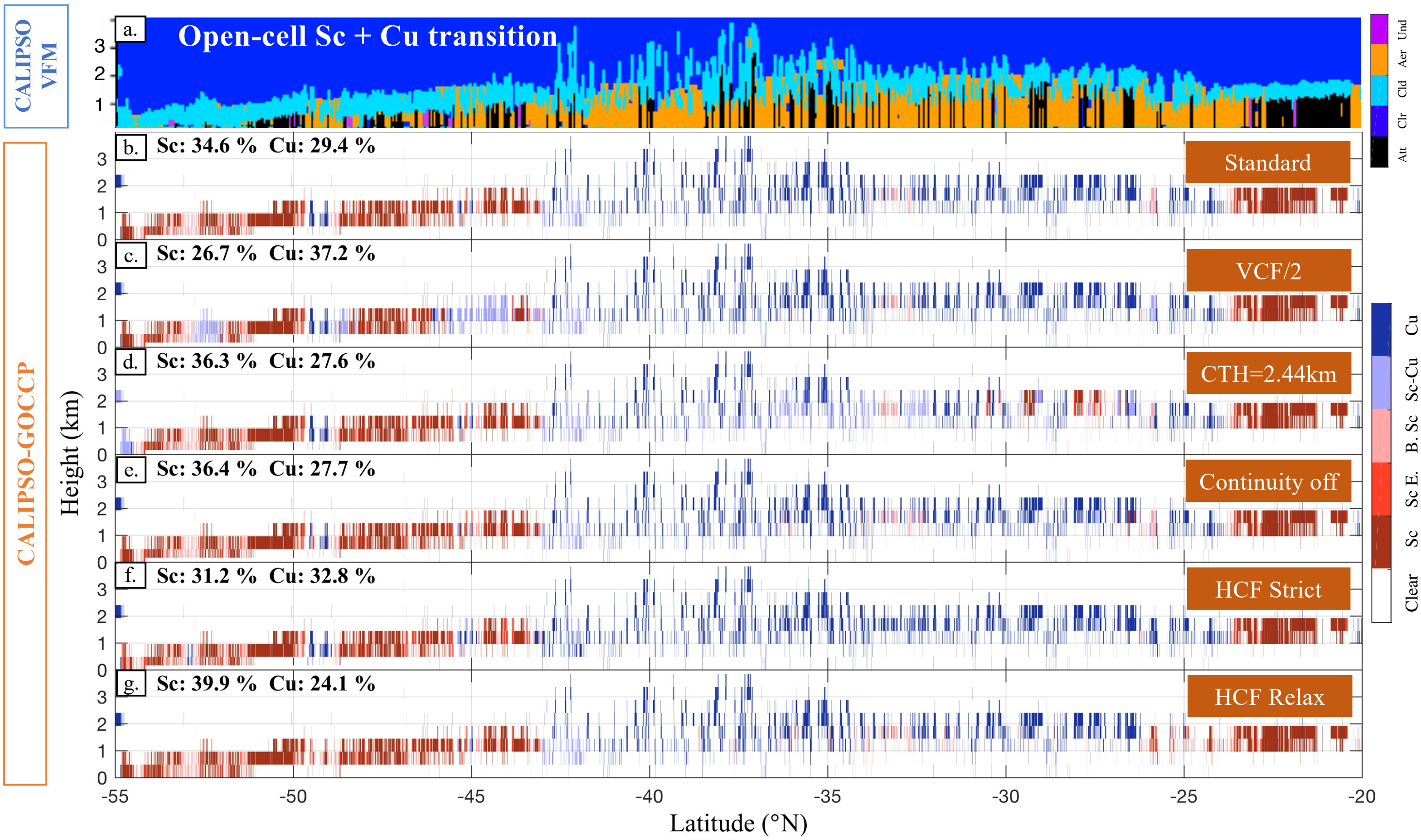

Earth Syst. Sci. Data Discuss., https://doi.org/10.5194/essd-2019-73
Manuscript under review for journal Earth Syst. Sci. Data
Discussion started: 22 May 2019

Figure 12: Same as Fig. 6 but for a typical Open-cell Sc to Cu transitioning case overlapping the south-east Pacific and the Southern Ocean (~ 55˚S to 20˚S, 2008-07-14 21:10:19, daytime).

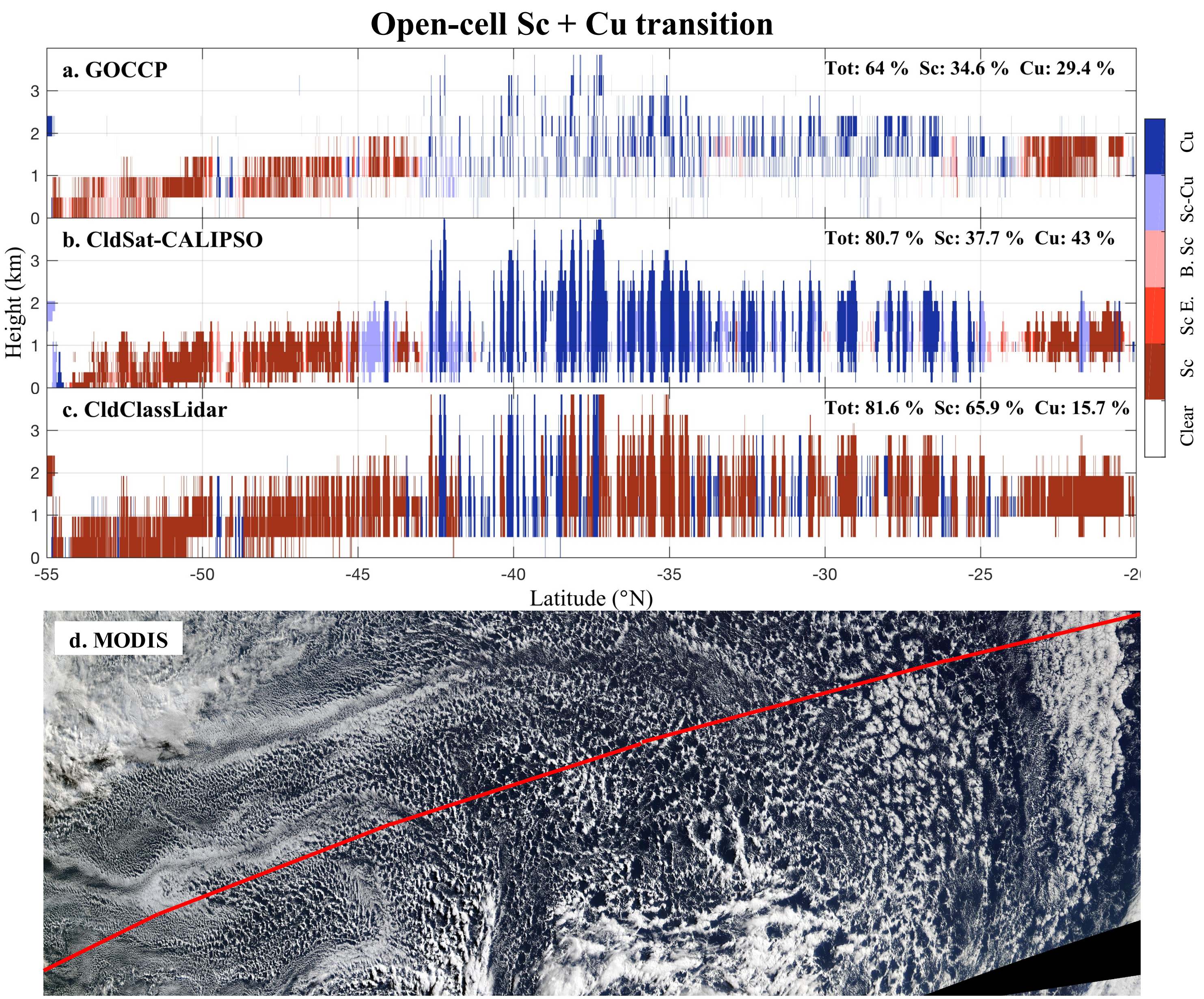

Earth Syst. Sci. Data Discuss., https://doi.org/10.5194/essd-2019-73
Manuscript under review for journal Earth Syst. Sci. Data
Discussion started: 22 May 2019

Figure 13: Maps (x axis, longitude [°E]; y axis, latitude [°N]) of (top to bottom) low, Sc , Cu Sc-Cu transitioning and the ratio Sc to Sc-and-Cu cloud fraction (%) for (left to right) GOCCP (2007-2016), RL-GeoProf (2007-2010), 2BCCL (2007-2010), MISR (2003-2012), MODIS Terra and Aqua (2003-2015) and ISCCP (1983-2008). Different color bars are used to better separate each type of cloud. Note that for active-sensor satellites, the low category accounts for all clouds present below 3.36 km regardless of their cloud top height, hence the sum of Sc, Cu and transitioning cloud fraction can be smaller than the low cloud fraction.

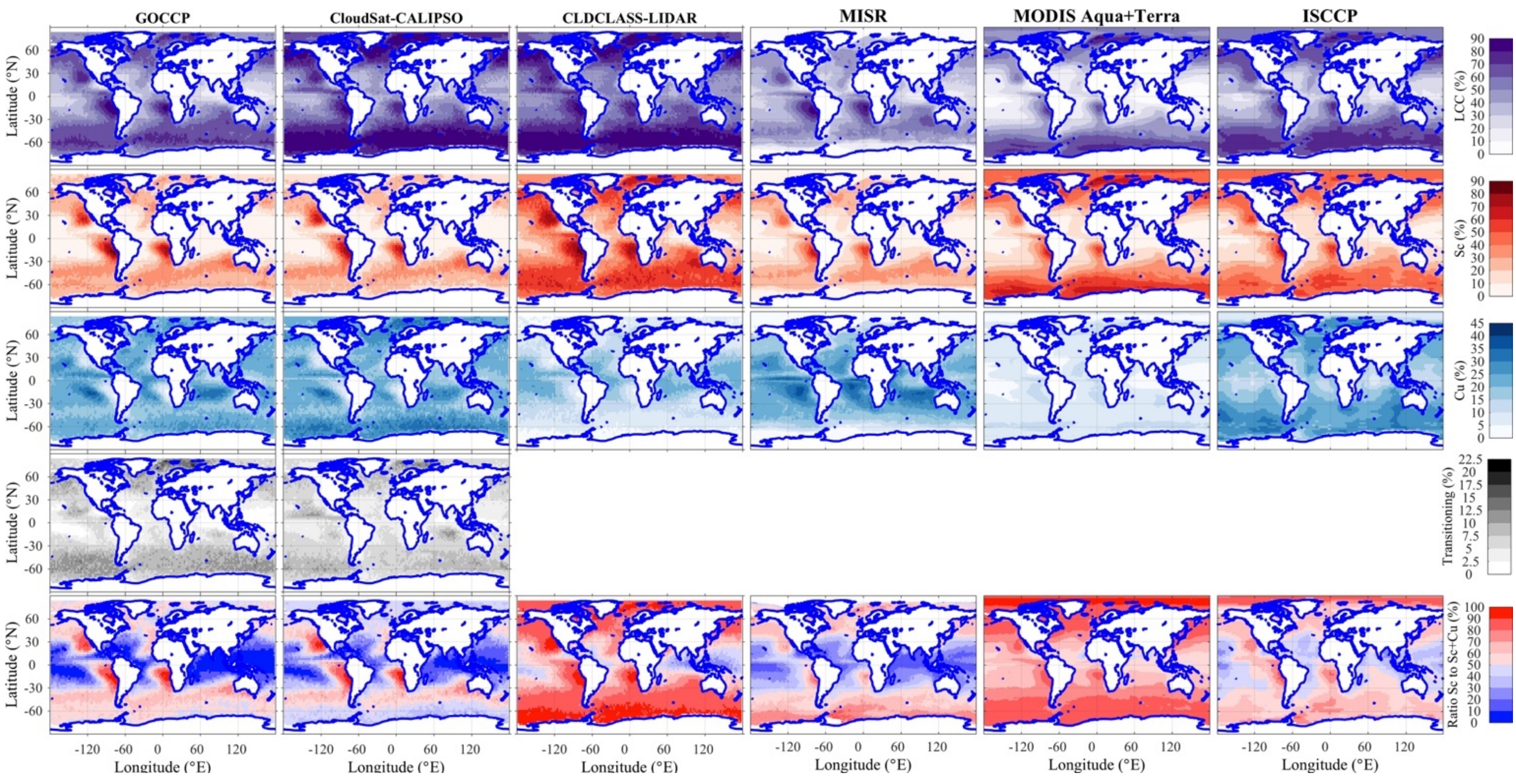

Earth Syst. Sci. Data Discuss., https://doi.org/10.5194/essd-2019-73
Manuscript under review for journal Earth Syst. Sci. Data
Discussion started: 22 May 2019

Figure 14: Global PDF (left), zonal mean (%, middle) and global area-weighted mean (%, right) of low, Sc, Cu, Sc-Cu transitioning and the ratio Sc to Sc-Cu clouds –from the top to the bottom– for all the satellite datasets using the same time period as in Fig. 13. Active-sensor observations are represented in solid lines as opposed to dashed lines for passive-sensor observations. Note that the y-axis are different in every subplots.

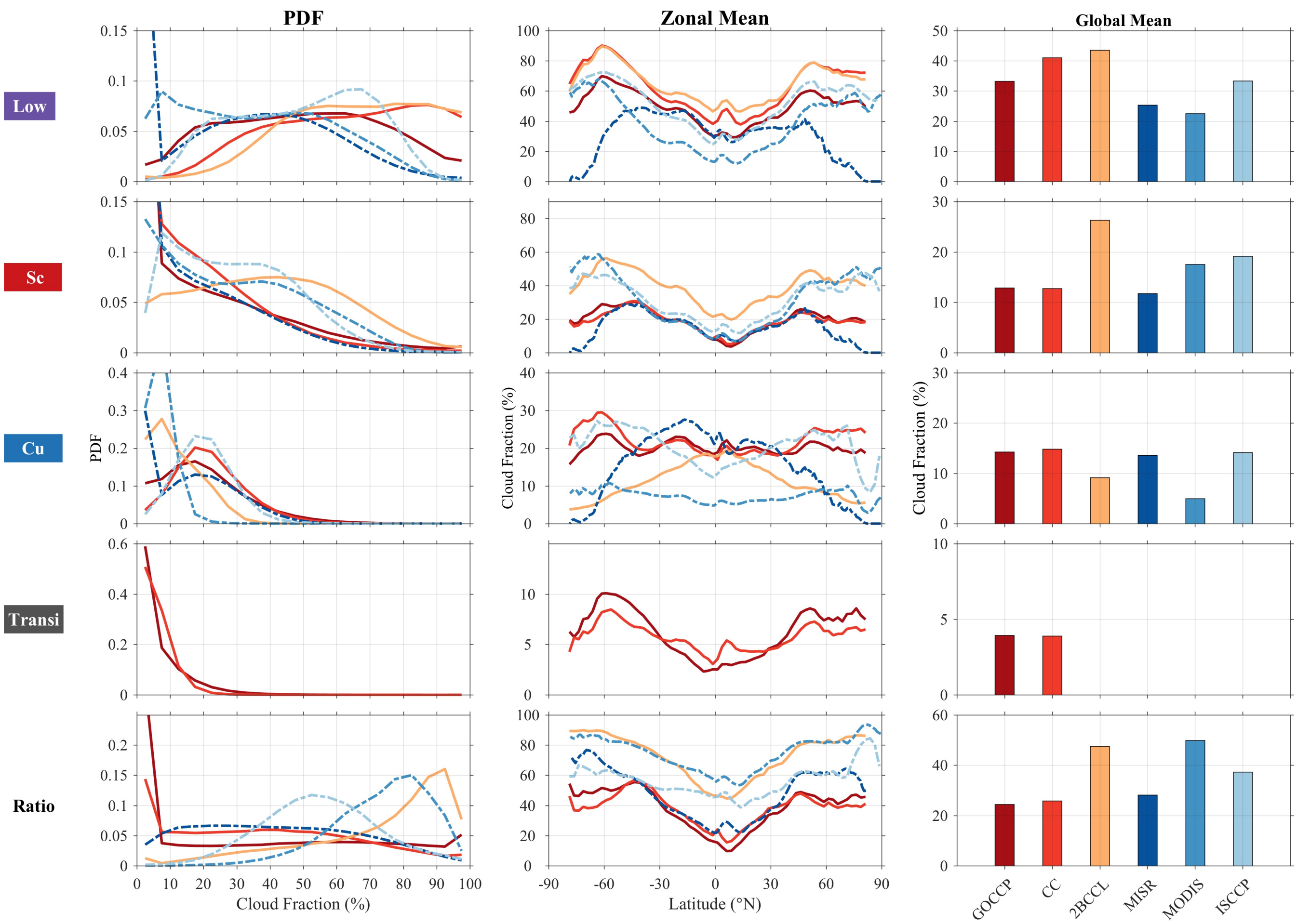

Earth Syst. Sci. Data Discuss., https://doi.org/10.5194/essd-2019-73
Manuscript under review for journal Earth Syst. Sci. Data
Discussion started: 22 May 2019

Figure 15: Zonal profiles (x axis, latitude [°N]; y axis, height [km]) of low (first row), Sc (second row), Cu (third row) and Sc-Cu transitioning (fourth row) cloud fraction (%) for GOCCP (first column), RL-GeoProf (second column) and 2BCCL (third column). As in Fig. 13, different color bars are used to better separate each type of cloud. The corresponding profiles for tropical subsidence regimes (ω500 > 10 hPa/day between 35°S/N following Cesana et al., 2019a) are represented in the fourth column for GOCCP (solid line), RL-GeoProf (dashed line) and 2BCCL (dotted line). Note that extratropical profiles are shown in Fig. S6.